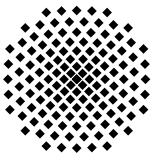

Universität Stuttgart - Institut für Wasser- und Umweltsystemmodellierung
Lehrstuhl für Hydromechanik und Hydrosystemmodellierung
Prof. Dr.-Ing. Rainer Helmig

Master's Thesis

Implementation of advanced algebraic turbulence models on a staggered grid

Submitted by
Priyam Samantray

Stuttgart, July 31, 2014

Examiners: Prof. Dr.-Ing. Rainer Helmig
Supervisor: Thomas Fetzer
Christoph Grüninger

I hereby certify that I have prepared this thesis independently, and that only those sources, aids and advisors that are duly noted herein have been used and/or consulted.

Stuttgart, July 31

Priyam Samantray

Acknowledgements

I express profound sense of gratitude to Thomas Fetzer for providing me indispensable assistance throughout the course of my thesis work. With his support, the project was approached in a systematic manner which lead to better understanding of the work. Also, I am highly indebted to Christoph Grüninger for his mature and critical comments at every stage of work.

Abstract

In natural science as well as in a lot of technical applications, turbulence is a phenomena which strongly influences flow and transport behavior. In contrast to laminar flow, the simulation of turbulent flow requires advanced numerical techniques. Even for small problems, a direct numerical simulation with the Navier-Stokes equations would be computationally too expensive. This can be solved by time averaging these equations, but then new equations for the eddy viscosity are required. The simplest solution is to calculate the eddy viscosity by algebraic relations. Additionally, using schemes like the vertex or cell centered finite volumes may lead to non-physical oscillations in the pressure field. Triggered by these facts, a different discretization scheme, called staggered-grid has been implemented in DuMu^x(www.dumux.org). In the scope of the proposed Master thesis, turbulence models, like the Baldwin-Lomax (Baldwin and Lomax [1978]), Cebeci-Smith model (Cebeci and Smith [1974]) and modifications of the Prandtl mixing length model are implemented into the DuMu^x framework. Then the implementation is tested against suitable numerical or physical experiments like Laufer [1954] and interpreted in relation to the old discretization technique.

Contents

List of Figures

Nomenclature

Latin letters

A	area	[m^2]
$\tilde{A}$	coefficient matrix	
A^+	model constant	[-]
C_{CP}	model constant	[-]
C_{Kleb}	model constant	[-]
F_{wake}	model constant	[-]
D	Diffusion coefficient	[m^2/s]
g	gravity constant	[m/s^2]
F,f	function	
L_k	Kolmogorov microscale	[m]
l	length	[m]
m	mass	[kg]
N	number	[-]
Pr	Prandtl	[-]
p	pressure	[$kg/m.s^2$]
q	source/sink term	[m/s]
Re	Reynolds number	[-]
t	time	[s]
u	main flow velocity component	[m/s]
y_m	wall distance of the switching point	[-]
y	wall distance	[m]
u_t	friction velocity	[m/s]

Greek letters

α	phase index	
Δ	difference	
δ	boundary layer thickness	[m]
κ	Karman constant	[-]
μ	dynamic viscosity	[kg/m.s]
μ_t	dynamic eddy viscosity	[kg/m.s]
$\nu_{t_{inner}}$, $\nu_{t_{outer}}$	kinematic eddy viscosities of Cebecci-Smith and Baldwin-Lomax model	[kg/m.s]
ν	kinematic viscosity	$[\mathrm{m}^2/s]$
ν_t	kinematic eddy viscosity	$[\mathrm{m}^2/s]$
τ_w	wall shear stress	[Pa]
ρ	density	$[\mathrm{kg}/m^3]$
τ	shear stress	$[\mathrm{kg}/m.s^2]$
ω	vorticity	$[1/s]$
δ_v	velocity thickness	[m]

Subscripts and superscripts

d	related to diameter
max	maximum value
min	minimum value
α	phase index

Others

a	vector
$\tilde{A}$	tensor
$\overline{a}$	temporal average
$\mathrm{a}^{'}$	quantity fluctuation
Δ	Laplace operator
∇	nabla operator

Abbreviations

CFD	Computational fluid dynamics
DNS	direct numerical simulation
DuMu$^{\mathrm{x}}$	DUNE for Multi-{Phase, -physics, -component, -scale, ...} flow in Porous Media
DUNE	Distributed and Unified Numerics Environment
RANS	Reynolds-averaged Navier-Stokes equation
PDE	partial differential equation

Chapter 1

Introduction

I am an old man now, and when I die and go to heaven there are two matters on which I hope for enlightenment. One is quantum electrodynamics, and the other is the turbulent motion of fluids. And about the former I am rather optimistic.

- Horace Lamb -

1.1 Motivation

In physical problems, turbulence is a key factor which influences the transport and flow behavior. For example, in sedimentation processes turbulence has chief importance to the human environment. These include problems concerning sediment transport and sedimentation like uncontrolled sand transport in rivers, unwanted dust in living areas and dust in electronic devices [20]. The sediment transport behavior is based on simple and empirical formulas which are applicable only for simple and very specific cases. With these approaches, the error can reach dozens or hundreds of percentages. Therefore, advanced models of turbulence are necessary for achieving solution pertaining to sediment transport in short time with a higher accuracy. In contrast to laminar flow, the simulation of turbulent flow requires advanced numerical techniques. For example, the simulation of blood flow in the aorta is complicated owing to occurrence of both laminar and turbulent flows in it [16]. During the cardiac cycle, the normal laminar flow of the aortic blood flow can become unstable and undergo transition to turbulence, at least in pathological cases such as coarctation of the aorta where the vessel is locally narrowed. The coarctation results in formation of a jet with high velocity, which creates a transition to turbulent flow. Turbulence requires advanced mathematical or physical models in order to resolve the flow features.
Even for small problems a direct numerical simulation with the Navier-Stokes equations would be computationally too expensive. Turbulence causes formation of eddies at different length scales. Majority of the energy is contained in large-scale structure. The energy cascades from these large scale structure to smaller scale by an inertial and essentially inviscid mechanism. This process continues, creating smaller and smaller

structures which produce a hierarchy of eddies. Eventually this process creates large number of small structures so that viscous dissipation occurs. The scale corresponding to this phenomena is named as *Kolmogorov length scale*(η). The Kolmogorov length scale is given by

$$\eta = (\nu^3/\epsilon) \text{ , where } \epsilon \text{ is rate at which larger eddies supply energy.}$$

Also, for high Reynolds turbulence, k which represents the kinetic energy per unit mass of fluctuating turbulent velocity can be expressed as

$$\epsilon \sim \frac{k^{3/2}}{l}$$

A particular case is considered to highlight the computational effort that will be required in solving the problem by direct numerical simulation of Navier-Stokes equation. In order to solve all scales, the grid spacing in terms of number of nodes in x-direction has to be

$$n_x = \frac{l}{\eta} = \frac{l}{\nu^3/\epsilon^{1/4}} \sim \frac{l(k^{3/2}/l)^{1/4}}{\nu^{3/4}} \sim Re_T^{3/4} \xrightarrow{3D} n_{tot} = 10^{15} nodes, \quad Re_T = \frac{k^{1/2} l}{\nu}$$

A commonly used dimensionless term relating inertia and laminar forces as a ratio is termed as Reynolds number which gives an indication of the turbulence. The term Re_T is the turbulence Reynolds number[27]. In order to illustrate the computational effort in direct numerical simulation, $Re_T^{3/4}$ is assumed a value of 10^5. The number of nodes in x-direction is equivalent to the turbulence Reynolds number as can be seen in the above expression. Hence, the total number of nodes in three dimensions will be equal to $(Re_T^{3/4})^3$ which equals 10^{15} nodes.

$$n_{tot} = 10^{15} nodes$$

$$\Downarrow$$

$$10^{15}\text{nodes} \cdot 4\text{var/node} \cdot 8\text{Byte/var} = 32 \cdot 10^6 \text{ GB}$$

Each node will have four variables to be solved. Each variable further requires 8 bytes of memory. Therefore, the total memory required to solve a problem by direct method is very large with a value of 32GB. Hence, the computational effort increases significantly in direct simulation of the Navier-Stokes equation.

Most of what can be done theoretically has already been done and experiments are generally difficult and expensive. As computing costs have continued to decrease, CFD has moved to the forefront in engineering analysis of fluid flow. To lower the computational effort, a classical technique used is the application of an averaging or filtering procedure to the Navier-Stokes equations yielding new equations for a variable that is

smoother than the original solution. This is due to the procedure of averaging which removes the small scales or high frequencies of the solution [19]. Being smoother, the smallest scales are less than the Kolmogorov scale but comparable to cutoff length scale. Hence, the computational effort and complexities are lowered. The higher frequencies are not included in the computation but their influence is considered via the use of a statistical model. The new variable to be calculated is the eddy viscosity. The simplest solution is to calculate the eddy viscosity by algebraic relations. For this purpose, two algebraic models namely Baldwin-Lomax model and Cebeci-Smith models are implemented in this thesis. However, these models are implemented using staggered grid discretization scheme because it provides a strong coupling between the velocities and pressure, which helps to oscillations in the pressure and velocity fields.

1.2 Contents of Thesis

The thesis which involves implementation of the algebraic turbulence models contains five chapters. Chapter 2 describes the physics pertaining to the flow of fluids. In the chapter 3, the mathematical equations, discretization schemes and physical assumptions are discussed in detail. In chapter 4, the simulation results of the three modifications of Prandtl mixing length models alongwith the models i.e. Cebeci-Smith and Baldwin-Lomax using a staggered grid are analyzed and conclusions are drawn. Finally, in the last chapter, a brief description of conclusions and scope for future research works are discussed.

Chapter 2

Basics Of Fluids

Theory is the essence of facts. Without theory, scientific knowledge would be only worthy of the madhouse.

- Oliver Heaviside -

The chapter 2 describes the physics pertaining to the fluid flow and turbulence.

2.1 Fluid Definition

A fluid is any substance that deforms continuously when subjected to a shear stress, no matter how small. For example, if one imposes a shear stress on a solid block of steel as depicted in fig. 2.1(a), the block would not begin to change shape until an extreme amount of stress has been applied. But if we apply a shear stress to a fluid element, for example of water, we observe that no matter how small the stress, the fluid element deforms, as shown in fig. 2.1(b)[13].

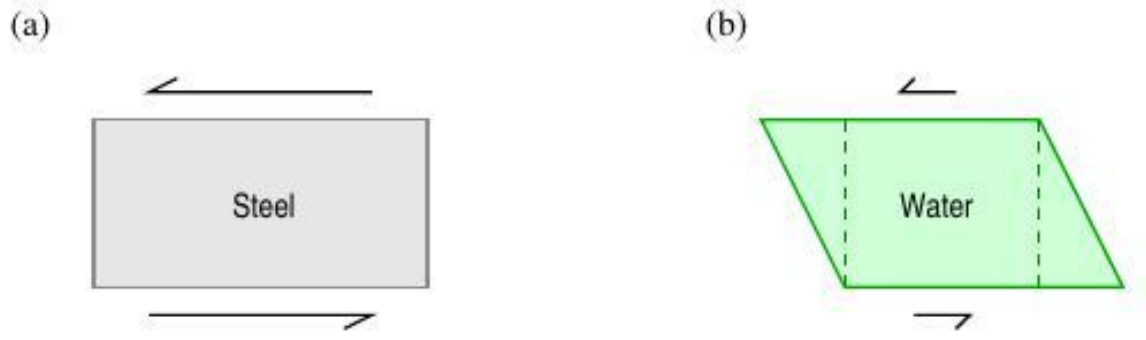

Figure 2.1: Deformation of fluid under shear force, from [13].

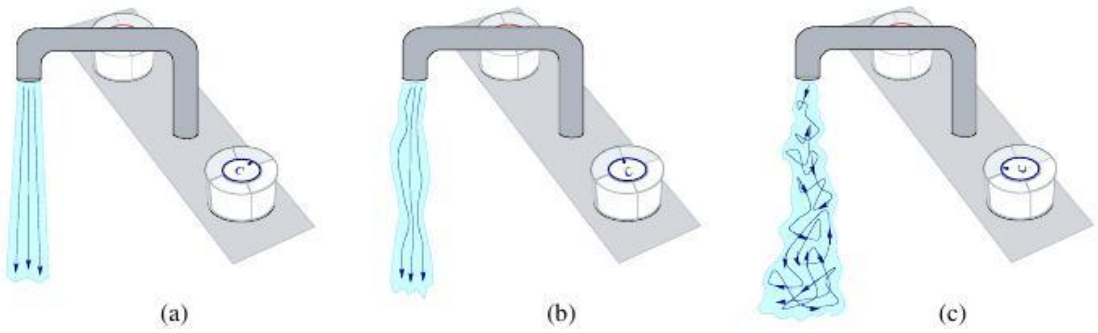

Figure 2.2: Laminar and turbulent flow of water from a faucet: (a) Steady laminar, (b) Periodic, wavy laminar, (c) turbulent, from [13].

2.2 Types Of Flows

Let us first define what a flow is: a flow is the continuous movement of a fluid, i.e. either a liquid or gas, from one place to another. Basically there exist two types of flows, namely laminar flows and turbulent flows as shown in fig. 2.2. In simple words, laminar flow can be stated as a simple flow while turbulent flow is a complicated flow.

2.2.1 Laminar Flow

Laminar flow, sometimes known as streamline flow, occurs when a fluid flows in parallel layers, with no disruption between the layers. Laminar flow occurs when the fluid is moving at a low velocity. The layers slide past one another but there is no lateral mixing. The motion of particles in fluid is very orderly with all particles moving in straight lines parallel to the pipe walls as can be seen in the fig. 2.3. It is a flow regime characterized by a low momentum convection but high momentum diffusion.

2.2.2 Turbulent Flow

In 1975, Hinze defined turbulence as an irregular condition of flow in which the various quantities show a random variation with respect to time and space coordinates as shown in fig. 2.3, so that statistically distinct average values can be discerned. The problem with this definition is the fact that non-turbulent flow can be described as irregular. The instantaneous properties in a turbulent flow are extremely sensitive to initial conditions but the statistical averages of instantaneous properties are not sensitive. However, in 1974, Bradshaw pointed that the time and length scales of turbulence are represented by frequencies and wavelengths. Some of the chief characteristics of the turbulent flows are briefly described in the following sections.

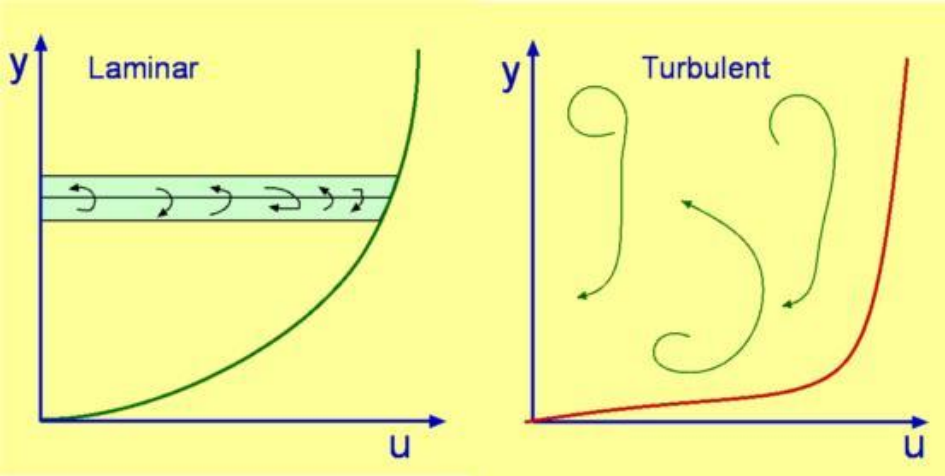

Figure 2.3: Velocity profiles of laminar and turbulent flows, from [5].

Instability The instability that develops in a laminar flow transforms into turbulence. Its occurrence can be attributed to the interaction between inertial terms and viscous terms.

Statistical aspects Since, turbulence is characterized by random fluctuations, it becomes necessary to use the statistical methods to analyze it. The time history of turbulent flow is stored and the required flow properties are integrated over the time to obtain the time averages.

Continuum phenomena of turbulence The smallest scales of turbulence are extremely small which are many orders of magnitude smaller than largest scales of turbulence. The ratio of smallest to largest scales decreases as Reynolds number increases.

Turbulence scales and cascade Turbulent flows comprises a continuous spectrum of scales ranging from largest to smallest. It can be visualized with eddies which can be described as a local swirling motion whose characteristic dimension is defined by the local turbulence scale. The eddies are loosely defined as coherent patterns of velocity, vorticity and pressure. The energy cascades from large scales to small scales by an inertial and inviscid mechanism. In this process, smaller eddies are created producing a hierarchy of the eddies. The larger eddies contain the smaller ones. Based on the length scales mentioned below, the eddies can be divided into three categories:

a) Integral length scale: These are largest scales in energy spectrum. These eddies obtain energy from mean flow and also from each other. These eddies contain most of the energy.

b) Kolmogorov length scales: Smallest scales in the spectrum that form the viscous sublayer range. They possess high frequency and cause the turbulence to be homogenous.

c) Taylor microscale: The intermediate scales between the largest and the smallest scales which make the inertial sub-range. These scales pass down the energy from largest to smallest eddies without dissipation [26].

In the energy cascade process, the kinetic energy transfer occurs from larger eddies to smaller eddies as the turbulence decays. The heat is dissipated by the smaller eddies through the action of viscosity. Therefore, the turbulent flows can be concluded as dissipative [27].

2.3 Relevant Flow Properties In Turbulence

2.3.1 Viscosity

Viscosity is the amount of internal friction or resistance of a fluid to flow. Water, for instance, is less viscous than honey, which explains why water flows more easily than honey. We consider flow between two horizontal parallel flat plates spaced at a distance 'h' apart, as depicted in fig. 2.4. A tangential force F is applied to the upper plate sufficient to move it at constant velocity U in the x direction, and study the resulting fluid motion between the plates.

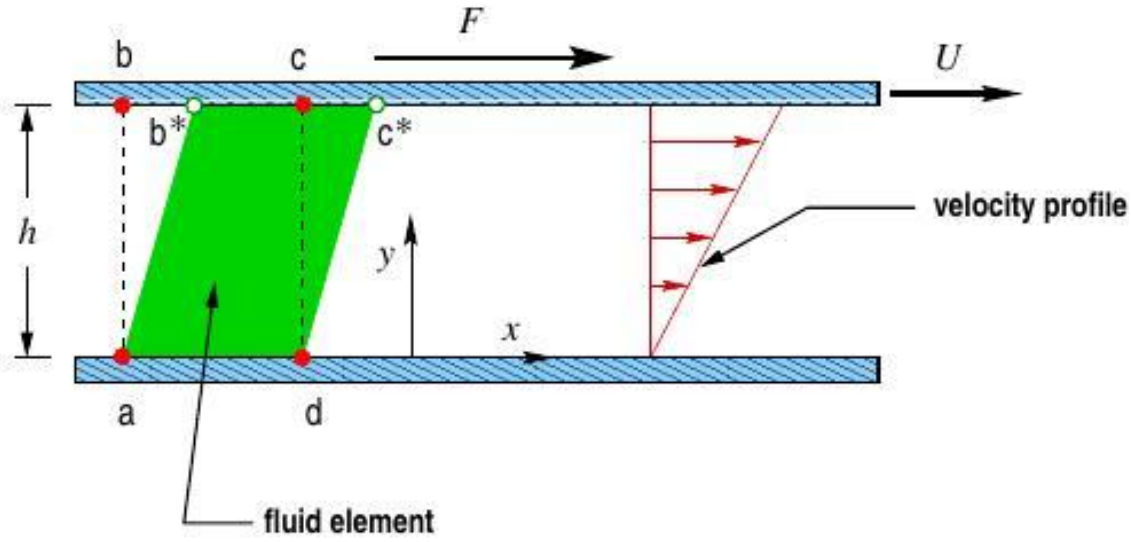

Figure 2.4: Flow between two horizontal, parallel plates with upper one moving at velocity U, from [13].

Experiments show that the force needed to produce motion of the upper plate with constant speed U is proportional to the area of this plate, and to the speed U. Furthermore, it is inversely proportional to the spacing between the plates, h. Thus, according to Newton's law of viscosity: For a given rate of angular deformation of a fluid, shear stress is directly proportional to viscosity.

$$F = \mu \frac{AU}{h} \tag{2.1}$$

Whether a flow is laminar or turbulent depends of the relative importance of fluid friction (viscosity) and flow inertia. The point at which laminar flow evolves into turbulent flow depends on other factors besides the velocity of the layers. A material's viscosity and specific gravity as well as the geometry of the Viscometer spindle and sample container all influence the point at which this transition occurs [1].

2.3.2 Velocity

It is worthwhile to note that an increase in velocity leads to a higher Reynolds number. And when the Reynolds number crosses a particular limit, the flow becomes turbulent. Moreover, for a turbulent flow the velocity components and other variables at a point fluctuate with time in an apparently random fashion. So, the velocity is considered as sum of an average value $\overline{u}(t)$ and random fluctuation $u^{'}$(t) as shown in fig. 2.5. This is known as Reynolds decomposition. Similarly, there is fluctuation in other variables like pressure and density.

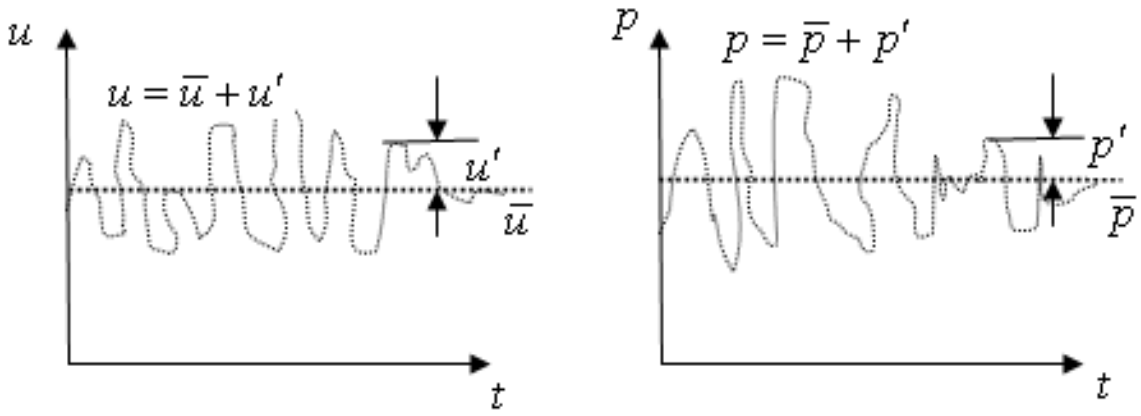

Figure 2.5: Velocity fluctuations in turbulent flow, from [15].

2.4 Boundary Layer

As the fluid passes around the object, molecules next to the surface stick to it. The speed of the molecules just above the surface gets reduced due to their collision with

the molecules sticking to the surface. The molecules just above the surface also slow down the flow that is just above them. However, as one moves away from the surface the reduction in speed of the molecules decreases. This creates a thin layer of fluid near the surface in which the velocity changes from zero at the surface to the free stream value away from the surface. This layer is called as boundary layer because it occurs on the boundary of fluid [9]. The aerodynamic boundary layer was first defined by Ludwig Prandtl(1904). The equations of fluid flow are simplified by dividing flow field into two areas i.e. one inside boundary layer where the viscosity dominates and the other outside the boundary layer with negligible viscosity effects. Hence, a closed form solution is obtained with simplification of the Navier-Stokes equations.

2.4.1 Laminar And Turbulent Boundary Layers

In a laminar boundary layer, any exchange of mass or momentum takes place only between adjacent layers on a microscopic scale. Consequently, the viscosity μ is able to predict the shear stress associated. Laminar boundary layers are found only when the Reynolds numbers are small. However, a turbulent boundary layer is marked by mixing across several layers of it on a macroscopic scale. Packets of fluid may be seen moving across. Thus there is an exchange of mass, momentum and energy on a much bigger scale compared to a laminar boundary layer.
A turbulent boundary layer is formed at only larger Reynolds numbers. The boundary layer thickness δ grows with distance from the leading edge. After some distance, from the leading edge, it reaches a constant thickness. This is termed as fully developed boundary layer.

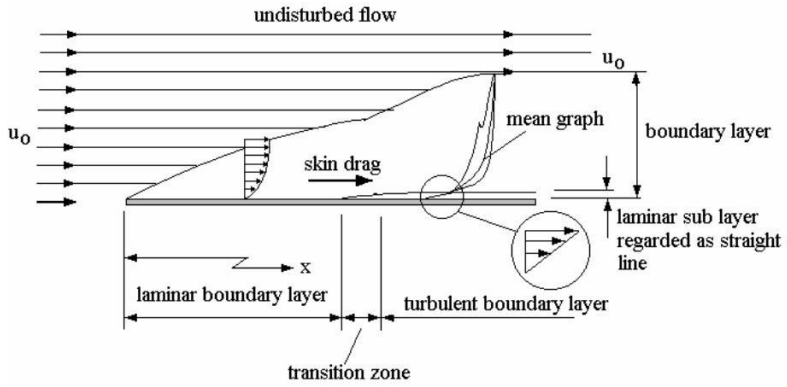

Figure 2.6: Boundary layer thickness, from [14].

Additionally, the boundary layer is divided into two layers namely turbulent boundary layer and viscous sublayer respectively after the flow becomes turbulent as noticed in fig. 2.6. It is worthwhile to note that the flow remains laminar in the viscous sublayer

as the viscous forces dominate in the region and near the wall which reduces the Reynolds number, even if the main flow is turbulent[24].

For laminar flows, the boundary layer thickness δ is small. For a flat plate, it is denoted as

$$\frac{\delta}{x} = \frac{5.0}{Re_x^{0.5}} \tag{2.2}$$

For turbulent flows, it is denoted as

$$\frac{\delta}{x} = \frac{0.385}{Re_x^{0.2}} \tag{2.3}$$

2.4.2 Some Terminology Of Boundary Layers

Thickness Of Velocity Boundary Layer It is defined as the distance from the solid body at which the viscous flow velocity is 99 % of the freestream velocity.

Displacement Thickness It is an alternative definition stating that the boundary layer represents a deficit in mass flow compared to inviscid flow with slip at the wall. Displacement thickness is defined as the distance by which the wall would have to be displaced in the inviscid case to give the same total mass flow as in viscous case [5].

2.4.3 Boundary Layer Transition

As the flow develops, the boundary layer thickens and becomes less stable and eventually becomes turbulent. This process is termed as boundary layer transition. When a fluid flows at high velocities, the boundary layer becomes turbulent and the gradient of the wall becomes smaller [17].

2.5 Measure Of Turbulence

A fluid makes a transition in its flow regime from laminar to turbulent as the inertial forces become more dominant than the viscous forces.
In the fig. 2.7, the Reynolds experiment is displayed which indicates the transition to turbulence of flow in a pipe as the flow speed is increased. As mentioned earlier, the magnitude of Reynolds number can give an indication regarding the turbulent or laminar regime of the fluid in consideration.
When the Reynolds number is small, the non-linearities are small, and we can solve the equation. In the fig. 2.8, it is observed that as the flow moves from left to right, we see the path of the dye streak generating more complicated patterns as the transition

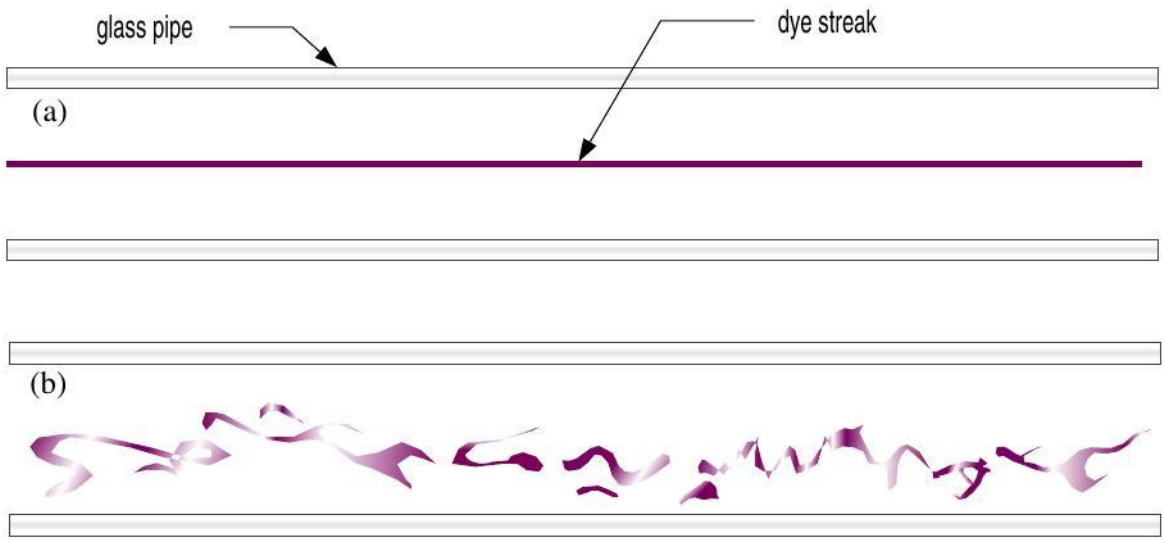

Figure 2.7: Reynolds' experiment using water in a pipe to study transition to turbulence; (a) low speed (b) higher-speed flow, from [13].

begins. Finally, the flow becomes turbulent in the extreme right region of pipe. In the turbulent flows, the non-linearities become more important. Eddies and vortices form and spin and dissolve without much obvious pattern.[13].

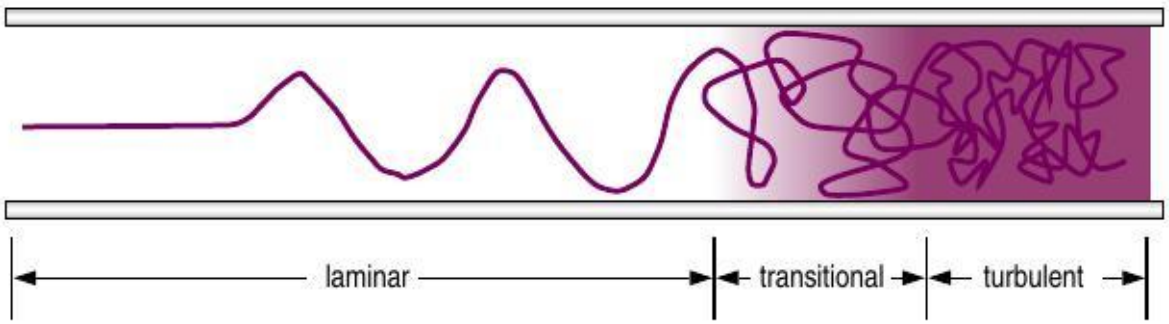

Figure 2.8: Transition to turbulence in spatially-evolving flow, from [13].

The flow in a pipe is laminar, transitional or turbulent provided the Reynolds number is small enough, intermediate or large enough. For general engineering purposes, the flow in a round pipe is laminar if the Reynolds number is less than approximately 2100. The flow in a round pipe is turbulent if the Reynolds number is greater than approximately 4000. For Reynolds number between these two limits, the flow may switch between laminar and turbulent conditions in random manner [11].

2.6 Law Of Wall And Turbulent Flow

According to the law of wall as mentioned by Theodore Von Karman, the average turbulent velocity at a particular point is proportional to the logarithm of the distance of the point under consideration from the wall. It is applicable to parts of the flow that are close to the wall ($< 20\%$ of the height of the flow). Dimensional analysis can be used to prove the logarithmic variation. A velocity scale u_t is defined which is derived from the surface shear stress τ_w. The velocity scale is expressed as

$$u_t = \sqrt{\frac{\tau_w}{\rho}} \tag{2.4}$$

The quantity u_t is also known as friction velocity which is a velocity scale representative of velocities close to a solid boundary.

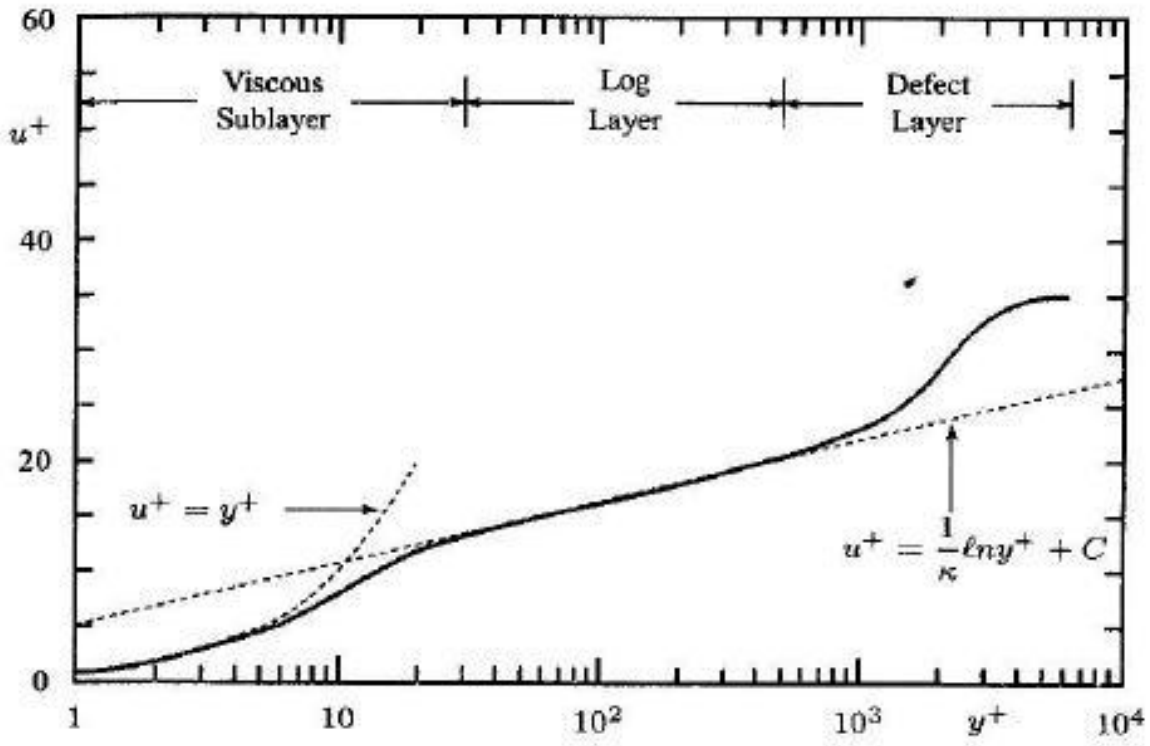

Figure 2.9: Velocity profile for a turbulent boundary layer, from [27].

The law of wall can be expressed as

$$\frac{U}{u_t} = \frac{1}{\kappa} \ln \frac{u_t y}{\nu} + C \tag{2.5}$$

Here κ is Karman constant, C is dimensionless integration constant, ν is kinematic

viscosity and U is the velocity at distance 'y' from wall respectively. The velocity profile for a turbulent layer is shown in fig. 2.9.
The dimensionless velocity u^+ and distance y^+ as observed in the fig. 2.9 are defined as

$$u^+ = \frac{U}{u_t}$$
$$y^+ = \frac{u_t y}{\nu} \tag{2.6}$$

Three distinct regions are observed namely viscous sublayer, log layer and defect layer. The velocity in viscous sublayer depends on u_t, ν and y. It can be represented in form of

$$U = u_t f(y^+) \tag{2.7}$$

where f(y+) is a dimensionless function. In the defect layer, a lot of experiments were performed by Darcy, von Karman and Clauser to obtain a suitable correlation with velocity-defect law or Clauser defect law which is expressed below:

$$U = U_e - u_t g(\eta),\ \eta \equiv \frac{y}{\Delta} \tag{2.8}$$

Here, U_e is the velocity at the boundary layer edge and $g(\eta)$ is a dimensionless function and Δ is a thickness characteristic of the outer portion of the boundary layer [27].

Chapter 3

Modelling The Turbulence

All models are approximations. Essentially, all models are wrong, but some are useful. However, the approximate nature of the model must always be borne in mind.

- George Edward Pelham Box -

In this chapter, the theory behind solving the turbulent flows and the relevant physical equations concerning fluids are discussed. Thereafter, the algebraic zero equation models for turbulence are described in detail. Furthermore, a brief outline about the numerical model implementing the staggered grid is discussed. Finally, the concepts and the structure of program used in implementation of the models are explained briefly.

3.1 Equations

The mathematical basis for a comprehensive general purpose model of fluid flow is formulated from the basic principle of conservation of mass, momentum and energy. In the conservation laws, the fluid is regarded as a continuum. In the formulation of equation for mass, momentum and energy, it is assumed that fluid is a continuous medium contained in a three dimensional space such that every parcel of the fluid, no matter how small in comparison with the whole body, can be viewed as a continuous material. For analysis of fluid flows at macroscopic length scales, the molecular structure of matter and the motions are ignored. The behavior of fluid is described in terms of macroscopic properties such as velocity, pressure, density and temperature and their space and time derivatives.

3.1.1 Mass Conservation

The mass conservation equation is derived with an assumption that the rate of increase of the mass in the fluid element is equal to net rate of flow of mass into fluid element. In the compact vector notation, it is denoted as

$$\frac{\partial \rho}{\partial t} = \frac{\partial(\rho u_i)}{\partial x_i} \tag{3.1}$$

3.1.2 Momentum Conservation

It is derived from the Newton's second law which states that the rate of change of momentum of a fluid particles equals the sum of all forces acting on the particle [18]. The equation of momentum conservation is stated as

$$\frac{\partial u_i}{\partial t} + u_j \frac{\partial u_i}{\partial x_j} = f_i - \frac{1}{\rho}\frac{\partial p}{\partial x_i} + \nu \frac{\partial^2 u_i}{\partial x_j \partial x_j} \tag{3.2}$$

where the vector f_i represents external forces.

3.2 Approaches

Turbulence simulation, in its purest form can be performed by Direct Numerical Simulation which is an entirely expensive approach requiring a millions of CPU hours for relevant Reynolds numbers as described earlier. However, another method known as Large Eddy simulation can be used. It models the effects of small eddies and resolves the large, most energetic eddies, the smallest resolved size being of order 10^2 of the appropriate dimension of the flow. Another way for resolving the time and space evolution of turbulence within a turbulent flow is achieved by a statistical approach which is followed in the current study. In this approach, integration of governing equations of flow in time and derivation of equations for time-averaged flow properties is performed so as to obtain the Reynolds-Averaged Navier-Stokes equations [10].

3.2.1 Reynolds Averaging

Three types of averaging are most relevant in turbulence modeling namely time average, spatial average and ensemble average. Time averaging is useful in turbulence which is stationary in nature i.e. the mean values does not vary with time. Let f(x,t) be an instantaneous flow variable. Its time average F_T(x) is defined as

$$F_T(x) = \lim_{T\to\infty} \frac{1}{T}\int_t^{t+T} f(x,t)\mathrm{d}x$$

Spatial averaging is used in turbulent flow that is uniform in all direction. The spatial coordinates are averaged. The average is denoted by F_v

$$F_V(t) = \lim_{V\to\infty} \frac{1}{V}\int_V f(x,t)\mathrm{d}V$$

Finally, the ensemble averaging used in turbulent modeling is most general type of Reynolds averaging suitable for flows that decay in time[27].

3.2.2 Reynolds -Averaged Navier-Stokes Equations (RANS)

As discussed earlier, the statistical approach is used for solving turbulent flows as there are often random fluctuations in the flow regime. In order to derive the Reynolds -Averaged Navier-Stokes Equations from the instantaneous Navier-Stokes equations, Reynolds decomposition is required. Reynolds decomposition refers to the splitting of flow variable (like velocity) into a mean component $\overline{u}(x)$ and fluctuating component $u^{'}$.

$$u(x,t) = \overline{u}(x) + u^{'}(x,t) \tag{3.3}$$

Some of the assumptions in derivation of Reynolds -Averaged Navier-Stokes Equations are as follows:
a) Constant viscosity
b) Density does not depend on pressure
c) The fluid in consideration is Newtonian
d) The fluid is incompressible
e) The mean values of turbulence does not vary with time

Assuming the fluid to be incompressible, the mass conservation equation reduces to

$$\frac{\partial u_i}{\partial x_i} = 0 \tag{3.4}$$

and the momentum equation is

$$\frac{\partial u_i}{\partial t} + u_j \frac{\partial u_i}{\partial x_j} = f_i - \frac{1}{\rho}\frac{\partial p}{\partial x_i} + \nu \frac{\partial^2 u_i}{\partial x_j \partial x_j} \tag{3.5}$$

Now, each of the instantaneous quantity is split into time-averaged and fluctuating components. The resulting equations are time-averaged yielding

$$\frac{\partial \overline{u}_i}{\partial x_i} = 0 \tag{3.6}$$

$$\frac{\partial \overline{u}_i}{\partial t} + \overline{u}_j \frac{\partial \overline{u}_i}{\partial x_j} + \overline{u_j^{'} \frac{\partial u_i^{'}}{\partial x_j}} = \overline{f}_i - \frac{1}{\rho}\frac{\partial \overline{p}}{\partial x_i} + \nu \frac{\partial^2 \overline{u}_i}{\partial x_j \partial x_j} \tag{3.7}$$

The momentum equation can be written as

$$\frac{\partial \overline{u}_i}{\partial t} + \overline{u}_j \frac{\partial \overline{u}_i}{\partial x_j} = \overline{f}_i - \frac{1}{\rho}\frac{\partial \overline{p}}{\partial x_i} + \nu \frac{\partial^2 \overline{u}_i}{\partial x_j \partial x_j} - \frac{\partial \overline{u_i^{'} u_j^{'}}}{\partial x_j} \tag{3.8}$$

Upon manipulating further, we obtain

$$\rho\frac{\partial\overline{u}_i}{\partial t}+\rho\overline{u}_j\frac{\partial\overline{u}_i}{\partial x_j}=\rho\overline{f}_i-\frac{\partial}{\partial x_j}\left[-\overline{p}\delta_{ij}+2\mu\overline{S}_{ij}-\rho\overline{u_i'u_j'}\right] \tag{3.9}$$

Here, μ is viscosity and the mean strain rate tensor s_{ij} is given by

$$s_{ij}=\frac{1}{2}\left(\frac{\partial u_i}{\partial x_j}+\frac{\partial u_j}{\partial x_i}\right) \tag{3.10}$$

Thus, the above equation represents the Reynolds averaged Navier-Stokes equation(RANS)[25]. The quantity -$\rho\overline{u_j'u_i'}$ is known as Reynolds stress tensor which is symmetric and has six unknown quantities. Thus, we have ten unknown variables in total i.e. one pressure and three velocity apart from the stress tensor. The total number of equations are four i.e. one mass conservation and three components of RANS. Hence, our system is not closed [27].

3.3 The Eddy Viscosity/Diffusivity Concept

The main idea behind Boussinesq's eddy-viscosity concept, which assumes that, in analogy to the viscous stresses in laminar flows, the turbulent stresses are proportional to the mean velocity gradient. So, the Boussinesq's hypothesis is used to model the Reynolds stress term. The Reynolds stress tensor is computed as a product of eddy viscosity and mean strain rate tensor [6].

$$\rho\overline{u_j'u_i'}=\mu_t\left(\frac{\partial\bar{u}_i}{\partial x_j}-\frac{\partial\bar{u}_j}{\partial x_i}\right)-\frac{2}{3}\left(K+\nu_t\frac{\partial\bar{u}_k}{\partial x_k}\right)\delta_{ij} \tag{3.11}$$

The above expression can be further written as

$$\rho\overline{u_j'u_i'}=2\nu_tS_{ij}-\frac{K}{\delta_{ij}} \tag{3.12}$$

where S_{ij} is the mean rate of strain tensor, ν_t is the turbulence eddy viscosity,
K = 1/2*$\rho\overline{u_j'u_i'}$ and δ_{ij} is the Kronecker delta [23].

However, to perform simple computations, the eddy viscosity is often computed in terms of mixing length which is analogous to the mean free path in a gas. The eddy viscosity depends on the flow of fluid. Therefore, the eddy viscosity and mixing length must be specified by an algebraic relation between eddy viscosity and length scales of the mean flow. The models comprising of algebraic relation are known as zero equation models i.e. Prandtl mixing length, Baldwin-Lomax and Cebeci-Smith are described in the corresponding sections.

3.4 Zero Equation Models

As mentioned earlier, the zero equation turbulence models implemented in the thesis work are the models which by definition do not require the solution of any additional equations and are calculated directly from the flow variables. These models are simple to use and helpful for simpler geometry. In 1925, Prandtl proposed the mixing length model for describing the momentum transfer by turbulent Reynolds stresses. Thereafter, three modifications of mixing length model was proposed by Van Driest (1956), Escudier (1966) and Corrsin and Kistler(1954) respectively.
Further, the concept of eddy-viscosity was even more developed by Cebeci and Smith (1967). Later, Baldwin and Lomax(1978) proposed an alternative algebraic model to eliminate some of the difficulty in defining a turbulence length scales from the shear layer thickness apart from incorporating the eddy-viscosity concept of Cebeci-Smith model. These models are discussed in the following sections.

3.4.1 Prandtl Mixing Length Model

In 1925, Prandtl proposed a mixing length hypothesis. The mixing length conceptually means that a fluid parcel will conserve its properties for a characteristic length, before mixing with the surrounding fluid. According to Prandtl, mixing length may be considered as the diameter of the masses of fluid moving as a whole in each individual case. He also defined the mixing length as the distance traversed by a mass of this type before it becomes blended with the neighboring masses [22]. He postulated the shear stress as

$$\tau_{xy} = \nu_t \left| \frac{\partial u}{\partial y} \right| \tag{3.13}$$

where the eddy viscosity, ν_t is given by

$$\nu_t = l_{\text{mix}}^2 \left| \frac{\partial u}{\partial y} \right| \tag{3.14}$$

The mixing length, $l = \kappa y$ with the Karman constant κ=0.40 or 0.41 and the distance from the wall y. This equation is valid only for wall bounded flows, additionally it is restricted to smooth surfaces. However, the model fails to provide close agreement with the measured skin friction for boundary layers. The mixing length relation is not expected to be constant throughout the boundary layer. Thus, several modifications to the equation have evolved which are described in the sections below [22].

3.4.2 Van Driest

Van Driest proposed the first modification of the Prandtl mixing length by multiplying the mixing length with a damping function. The expression for mixing length was an outcome of good fit to the data as it rendered some theoretical support.

$$l_{\text{mix}} = \kappa y \left(1 - e^{\frac{-y^+}{A_0^+}}\right) \tag{3.15}$$

After a series of experiments, the value of A_0^+ equal to 26 was found to give good results. The Van Driest modification improves the description of the Reynolds stress in the limit y $\rightarrow$ 0 [27].

3.4.3 Escudier Modification

In 1966, Escudier found that the predictive accuracy is improved by limiting the mixing length a certain value. The maximum value of the mixing length in the Escudier modification is given by

$$(l_{\text{mix}})_{\text{max}} = 0.09\ \delta$$

δ is boundary layer thickness. Escudier's modification is similar to the approximation that is used in analyzing the free shear flows [27].

3.4.4 Corrsin and Kistler Modifications

Corrsin and Kistler proposed a modification as a result of the corollary of their experimental studies of intermittency. It was found that upon approaching the free stream from within the boundary layer, the flow is sometimes laminar and turbulent i.e. it is intermittent. Hence, in this modification, the eddy viscosity is obtained by multiplying the eddy viscosity of the Prandtl mixing length model by the Klebanoff function which is given by

$$F_{\text{Kleb}}(y;\delta) = \frac{1}{\left[1 + 5.5\left(\frac{y}{\delta}\right)^6\right]} \tag{3.16}$$

The above expression gives measure of the effect of intermittency of flow [12].

3.4.5 Cebeci-Smith Model

This is a two layer model in which the boundary layer is considered to comprise an inner and an outer layer. The eddy viscosity is calculated separately for each layer and combined using

$$\nu_t = \begin{cases} \nu_{t_{\text{inner}}} & \text{if } y \leq y_m \\ \nu_{t_{\text{outer}}} & \text{if } y > y_m \end{cases}$$

where y_m is the smallest distance from the surface where $\nu_{t_{\text{inner}}}$ is equal to $\nu_{t_{\text{outer}}}$. The concept involving the calculation of y_m is explained in the later sections. The inner-region eddy viscosity is given by:

$$\nu_{t_{\text{inner}}} = l_{\text{mix}}^2 \sqrt{\left[\left(\frac{\partial U}{\partial y}\right)^2 + \left(\frac{\partial V}{\partial x}\right)^2\right]} \tag{3.17}$$

$$l_{mix} = \kappa y \left(1 - e^{\frac{-y^+}{A^+}}\right) \tag{3.18}$$

$$A^+ = \frac{26}{\sqrt{\left(1 + y\frac{\frac{dP}{dx}}{\rho u_\tau^2}\right)}} \tag{3.19}$$

The coefficient A^+ is different than the Van Driest value for an improvement of predictive accuracy in boundary layers with nonzero pressure gradient. The eddy viscosity in the outer region is given by:

$$\nu_{t_{\text{outer}}} = \alpha U_e \delta_v^* F_{Kleb} \tag{3.20}$$

where, α=0.0168, U_e is the boundary layer edge velocity and δ_v^* is the velocity thickness given by

$$\delta_v^* = \int_0^\delta \left(1 - \frac{U}{U_e}\right) \mathrm{d}y \tag{3.21}$$

For incompressible flows, it can be noted that velocity thickness is identical to displacement thickness [21]. The F_{Kleb} is the Klebanoff intermittency function given by

$$F_{\text{Kleb}}(y;\delta) = \frac{1}{\left[1 + 5.5\left(\frac{y}{\delta}\right)^6\right]} \tag{3.22}$$

The model is suitable for high-speed flows with thin attached boundary-layers, typically present in aerospace applications.

3.4.6 Baldwin-Lomax Model

In 1978, Baldwin and Lomax formulated a two layer algebraic equation model. It is used in applications where the parameters like boundary layer thickness δ, velocity thickness δ_v^* cannot be easily determined. Similar to the Cebeci-Smith, this model uses inner and outer layer eddy viscosity [6]. The inner and outer viscosity are selected

in a similar criteria like the Cebeci-Smith model.

Here, again y_m is defined as the smallest distance from the surface where $\nu_{t_{\text{inner}}}$ is equal to $\nu_{t_{\text{outer}}}$. Similar concept is adopted in calculation of the value of y_m which is discussed in the later sections. The inner viscosity is given by

$$\nu_{t_{\text{inner}}} = (l_{\text{mix}})^2|\omega|$$

where , ω = magnitude of the vorticity vector in three dimensions. The vorticity parameter is used instead of the velocity gradient for determination of the eddy viscosity. The mixing length is calculated by Van driest equation

$$l_{mix} = \kappa y \left[1 - e^{-y^+/A_0^+}\right] \tag{3.23}$$

The outer viscosity is given by

$$\nu_{t_{\text{outer}}} = \alpha C_{\text{cp}} F_{\text{Wake}} F_{\text{Kleb}}(y; y_{\text{max}}/C_{\text{Kleb}}) \tag{3.24}$$

where, $F_{\text{wake}} = \min\ (y_{\text{max}} F_{\text{max}};\ C_{\text{wk}} y_{\text{max}} U_{\text{dif}}^2 / F_{\text{max}})$

$F_{\text{max}} = \frac{1}{\kappa}\,(\max(l_{\text{mix}}|\omega|))$

where, F_{max} is maximum value of $l_{mix}|\omega|$ and y_{max} is the distance at which this maximum occurs for a given x-position. Here, α=0.0168, C_{cp}= 1.6, C_{Kleb}=0.3, C_{wk}=1, κ =0.40 and A_0^+=26 respectively.

In this model there is no need to locate the boundary layer edge by calculating the outer layer length scale in terms of the vorticity instead of the displacement. By replacing $U_e\delta_v^*$ in the Cebeci-Smith model by $C_{\text{cp}}F_{\text{Wake}}$, we have

A) If $F_{\text{Wake}} = y_{\text{max}}F_{\text{max}}$ *then* $\delta_v^* = \frac{y_{max}^2\omega}{U_e}$

B) If $F_{\text{Wake}} = \frac{C_{\text{wk}}y_{\text{max}}U_{\text{dif}}^2}{F_{\text{max}}}$ *then* $\delta = \frac{U_{dif}}{|\omega|}$

An important observation for pipe and channel flow is that subtle difference in a model's prediction for Reynolds stress can lead to much larger differences in velocity profile predictions. This is a common accuracy dilemma with many turbulence models. Both Cebeci-Smith and Baldwin-Lomax models have been fine-tuned for boundary layer flow and therefore provide good agreement with experimental data for reasonable pressure gradients and mild adverse pressure gradients.

3.5 Numerical Model

After the derivation of the relevant mathematical equations mentioned earlier, a numerical model is implemented to solve the developed equations. This is because the equations are coupled and non-linear partial differential equations. These can be solved by using the discretization schemes in space and time in a numerical model. Therefore, a numerical simulator named as DuMu^x is used in the thesis to solve the equations and obtain the results [4].

3.5.1 DuMu^x

DuMu^x is a generic framework which is used for simulation of multiphase fluid flow and transport processes in porous media by the application of continuum mechanical approaches. DuMu^x models the concepts, constitutive relations, discretizations and solvers. Its objective includes delivering top computational performance, high flexibility, ability to run on single processor systems and highly parallel supercomputers. It has C++ as its implementation language.

DuMu^x provides a framework for easy implementation of problems concerning porous media flow problems with a variety of selection of spatial discretization schemes, temporal discretization schemes and nonlinear solvers along with the concepts of model coupling.

DuMu^x is a module of DUNE (the Distributed and Unified Numerics Environment). DUNE provides an interface to many existing grid management libraries. It also provides set of finite element functions and routines for solving partial differential equations [7].

3.5.2 Box method

In a previous study, the box method of discretization was used to model the turbulent flows. In this method, the model domain is discretized with a finite element mesh of nodes and elements. Thereafter, a secondary mesh is created by connecting the midpoints and barycenteres of the elements surrounding the node to form a box around it. The finite element mesh divides the box into subcontrol volumes. The finite volume method is applied to each box so as to obtain the fluxes across the interfaces at the integration points from the finite element approach.
This method uses the benefit of finite element method which can be used with unstructured mesh and of finite volume method which is mass conservative. In the later section of study, the results of box method are compared with the staggered grid to draw some conclusions.

3.5.3 Discretization In Space Using Staggered Grid

In the current study, a staggered grid discretization method is adopted in the problem so as to prevent the occurrence of pressure oscillations. In this step, the problem geometry is split into finite number of volumes. In the cell centered finite volume method, the pressure and velocities are defined at the nodes of an ordinary control volume.

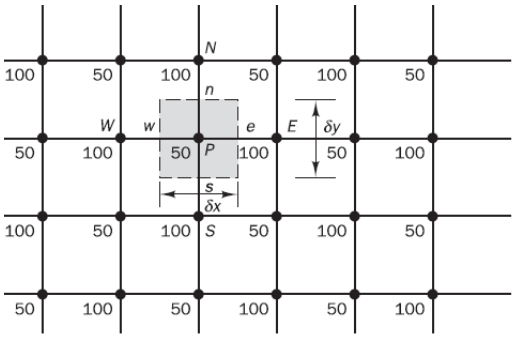

Figure 3.1: A checker-board pressure field, from [18].

$$\frac{\partial p}{\partial x} = \frac{p_e - p_w}{\delta x} = \frac{\left(\frac{p_E + p_W}{2}\right) - \left(\frac{p_P + p_W}{2}\right)}{\delta x} = \frac{p_E - p_W}{2\delta x} \tag{3.25}$$

In the fig. 3.1, it is found that the discretized pressure gradients in equation 3.25 have a zero value at all the nodal points in spite of the pressure field exhibiting spatial oscillations in both directions. This would render zero momentum source in the discretized equations. This behavior is absolutely unphysical. Moreover, if the velocities are also represented in grid nodes, the effect of pressure is not evident in momentum equations. In order to solve the existing problem, a staggered grid is used.

For a staggered grid, the cell centered finite volume method is used for discretization of the pressure at the center of control volume. The control volume is formed by the elements of the grid. However, the velocities are defined at the cell faces in between the nodes i.e. shifted by half the value of a cell and are indicated by arrows.
In the staggered grid arrangement shown in fig. 3.2, the pressure nodes coincide with the cell faces of u-control volume. The pressure gradient term is given by

$$\frac{\partial p}{\partial x} = \frac{p_P - p_W}{\delta x_u} \tag{3.26}$$

The checker board field with staggered grid arrangement is considered again and the appropriate nodal pressure values are substituted in the (3.26). This yields non-zero values of pressure in x-direction.
Thus, the staggering of the velocity components prevents an unrealistic behavior of

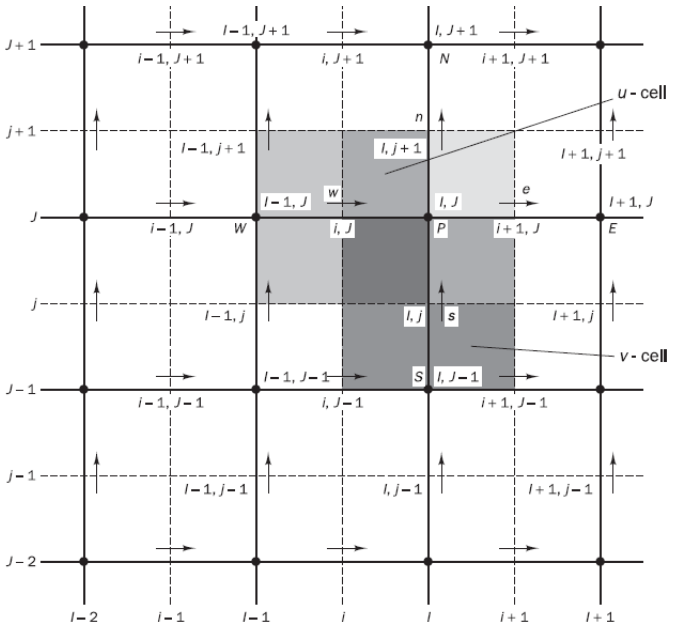

Figure 3.2: A staggered grid arrangement, from [18].

the discretized momentum equation due to oscillating pressure values. Moreover, the velocities are obtained at exactly the locations where they are required for the scalar transport [18].

3.5.4 Discretization in time

In the thesis, an implicit time stepping scheme is used for time discretization. The equations are solved for primary variables at new time level t_{i+1}. The current time level is represented as t_i [2]. The storage term of each balance equation is given by

$$\frac{\partial u}{\partial t} \approx \frac{u^{i+1} - u^i}{t_{i+1} - t_i} = \tilde{A}^{i+1} u^{i+1} \tag{3.27}$$

Here, the vector u contains the unknowns and the $\tilde{A}$ is the coefficient matrix. The implicit method is adopted as it is unconditionally stable [3].

3.6 Notes on Implementation

In the implementation of the algebraic models, the knowledge of certain properties among all the elements in a particular column of the discretized domain of flow is required.

3.6.1 General Notes

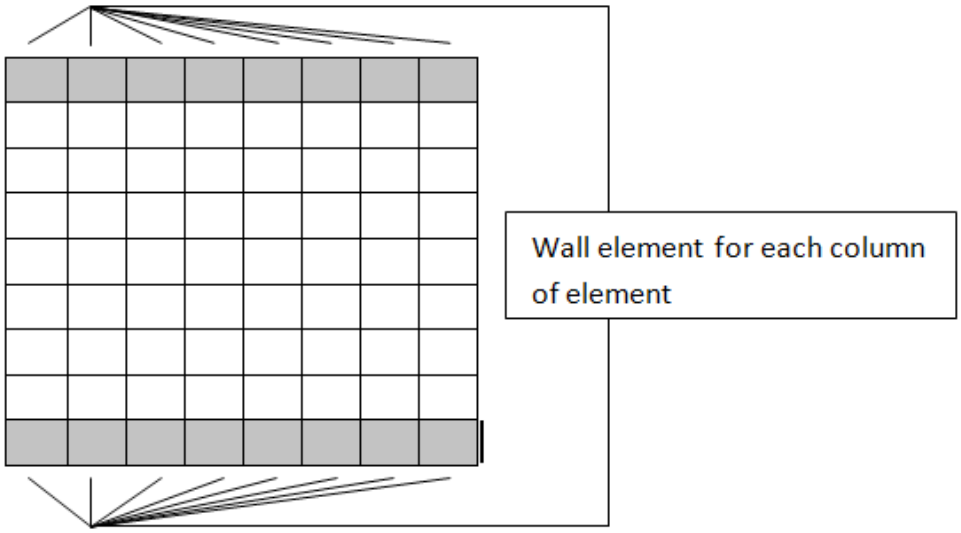

Figure 3.3: Wall elements in a domain.

In the program, at the beginning of a time step, the maximum velocity is evaluated among all elements of each column. The wall element in the discretized domain is shown in the fig. 3.3. The value of maximum velocity is stored at the upper or lower wall element in each column. It depends on the closeness of the element to the wall in that column. If the element containing maximum velocity is close to the bottom wall as compared to the upper wall, then the maximum velocity will be stored in bottom wall and vice-versa. Since, the problem under consideration is symmetric in nature, the same values of maximum velocities are obtained for the same column.
The maximum velocity so obtained is essential to calculate the boundary layer thickness and Reynolds number which are required in implementation of the 2nd and 3rd modification of the Prandtl mixing length models, Cebeci-Smith and Baldwin-Lomax models.

3.6.2 Concept in Implementation of the Cebeci-Smith and Baldwin-Lomax Model

In the Cebeci-Smith model, it is required to obtain the values of y_m so as to assign the eddy viscosity a value equal to the inner or outer viscosity as discussed earlier. y_m is defined as the distance from the wall where the inner viscosity is equal to outer viscosity. So, the value can be determined by equating these viscosities and

solving for y_m. However, solving in this manner is not easy due to complex nature of the expressions for the viscosities. Therefore, another approach is adopted for computation of y_m. In this approach, the difference between both the viscosities are determined for each element in the column. If the viscosities are equal, their difference will be zero. Therefore, the aim is to search for elements in the column having lowest value of this difference. However, it may be difficult to get a zero value. Therefore, even the lowest absolute value of difference is also considered.

$$\Delta\nu = \min(\nu_{t_{\text{outer}}} - \nu_{t_{\text{inner}}}) \tag{3.28}$$

In the program, the difference between both viscosities is named as compi. If the value of compi for the next element in the same column is less than stored least value, then compi is assigned this lesser value. The least value of compi among all elements in each discretized column is stored in the wall element of the corresponding column. Finally after evaluating all the elements, the wall distance of the element having least value of compi in each column is assigned as y_m for the corresponding column of elements. Thereafter, the eddy viscosity is determined for further computations.

Similar approach is adopted in the computation of y_m for Baldwin-Lomax Model.

3.6.3 Structure of the Program

The program is created implementing the algorithm for the three modifications of the Prandtl mixing length model, the Cebeci-Smith and Baldwin-Lomax model. The structure of the programs are explained in a convenient manner through a schematic representation i.e. for the three modifications, Cebeci-Smith Model and Baldwin-Lomax model.

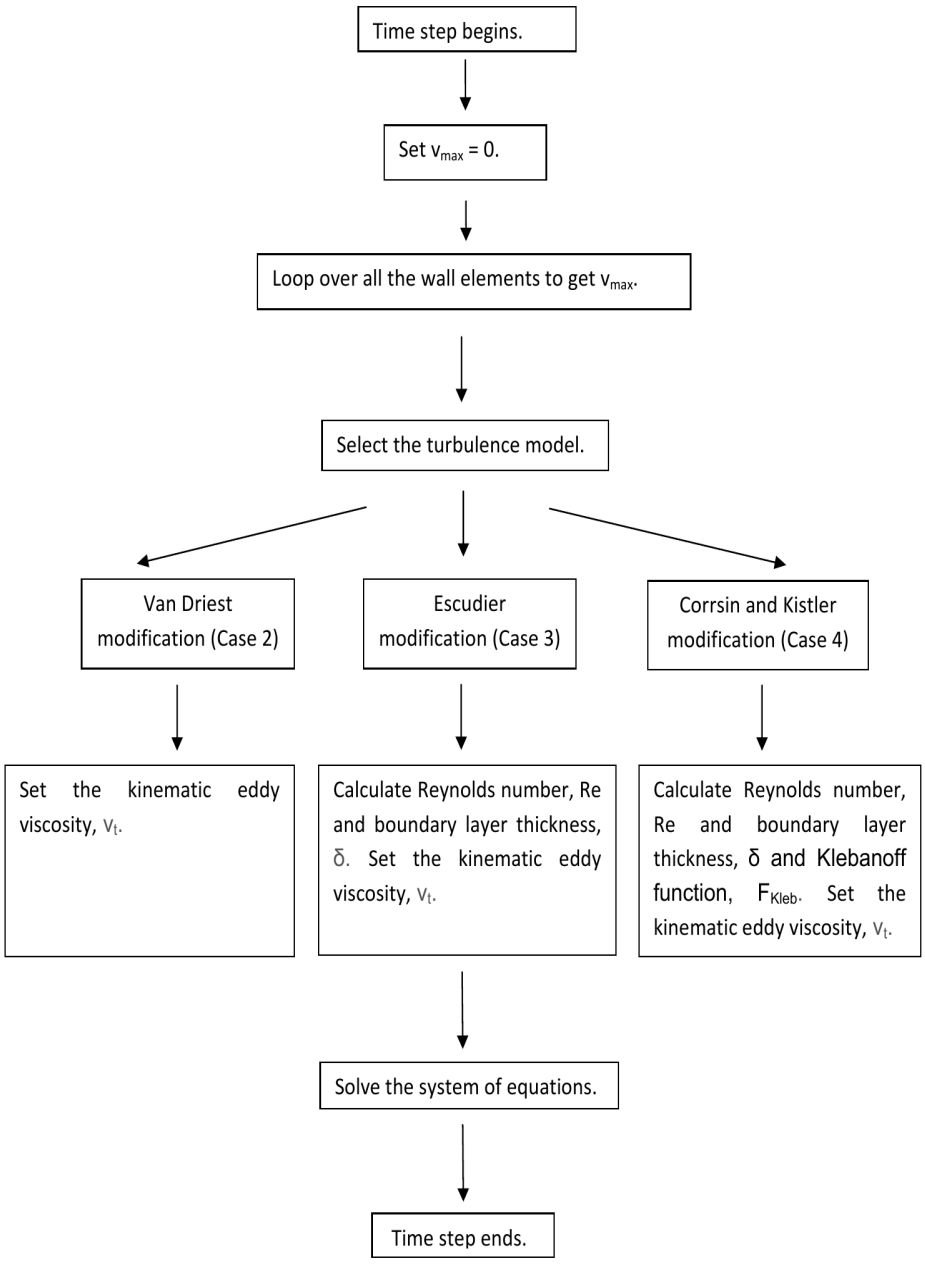

Figure 3.4: Structure of program for computation implementing three modification of Prandtl Mixing Length model.

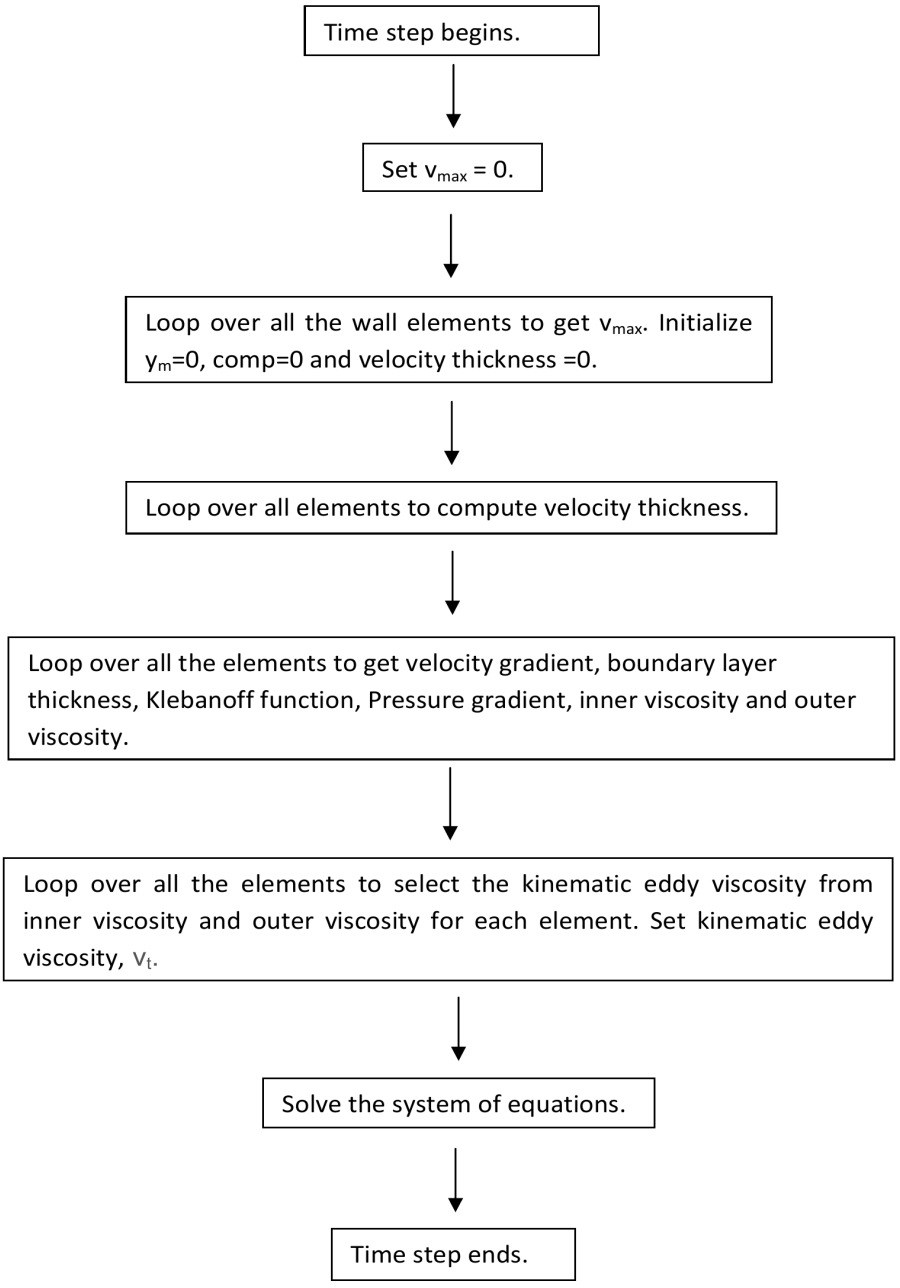

Figure 3.5: Implementation of the Cebeci-Smith Model.

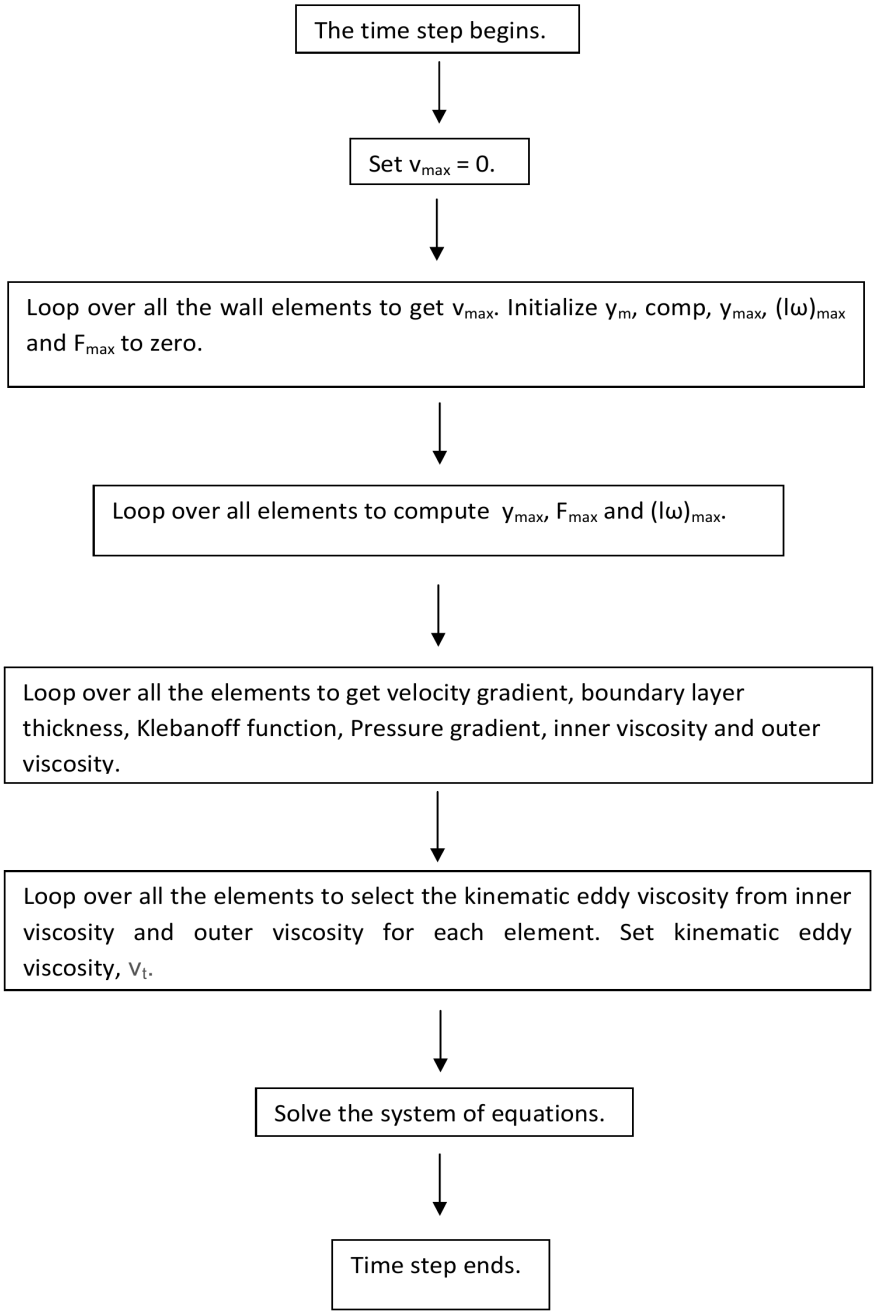

Figure 3.6: Implementation of the Baldwin-Lomax Model.

Chapter 4

Results and Discussion

We must trust to nothing but facts: These are presented to us by Nature, and cannot deceive. We ought, in every instance, to submit our reasoning to the test of experiment, and never to search for truth but by the natural road of experiment and observation.

- Antoine Lavoisier, Elements of Chemistry -

In this chapter, the results are computed for a set of input parameters. Thereafter, the results are obtained and analyzed for different cases. The analysis is performed in two ways i.e. Analysis of each model Individually and Comparative analysis of all the models. Finally, conclusions are derived based on the results.

4.1 Model Description

In the current work, the pipe is modeled in a two dimensional domain. The computation of the zero equation models were performed using standard values of the parameters as depicted below in the table.

Length	**Thickness**	**Low velocity**	**Density**	**Kinematic viscosity**	**Time step**
10m	0.2469m	2.5m/s	1.21kg/cm^3	10^{-6}m^2/s	0.1s
End time	**Pressure**	**Low Re**	**High Re**	**High velocity**	
7s	10^5Pa	50 000	500 000	25m/s	

The discretized cells that are considered range from values of 16 to 64 in each direction for the problem. The inflow and initial velocity are constant over height, but set to zero at the upper and lower boundaries, which is called no slip condition. This ensures the momentum balance. On the right side of pipe, the velocity is set as an outflow condition. On the right boundary the pressure is set as Dirichlet condition so as to maintain mass balance.

4.2 Individual Analysis

In this section, an effort is made to understand the fundamental characteristics of each model through their outputs. The input values discussed earlier are used in performing computations for all the models in this section.

4.2.1 Van Driest Modification

The Prandtl mixing length model does not approximate the viscous sub layer properly especially at the wall. It considers the eddy viscosity in the viscous sublayer uniformly. The eddy viscosity becomes zero only at the wall where $y^+ = 0$. However, Van Driest made the eddy viscosity decrease exponentially as one nears the wall through the damping function instead of switching it on in the turbulent and sublayer regions respectively.

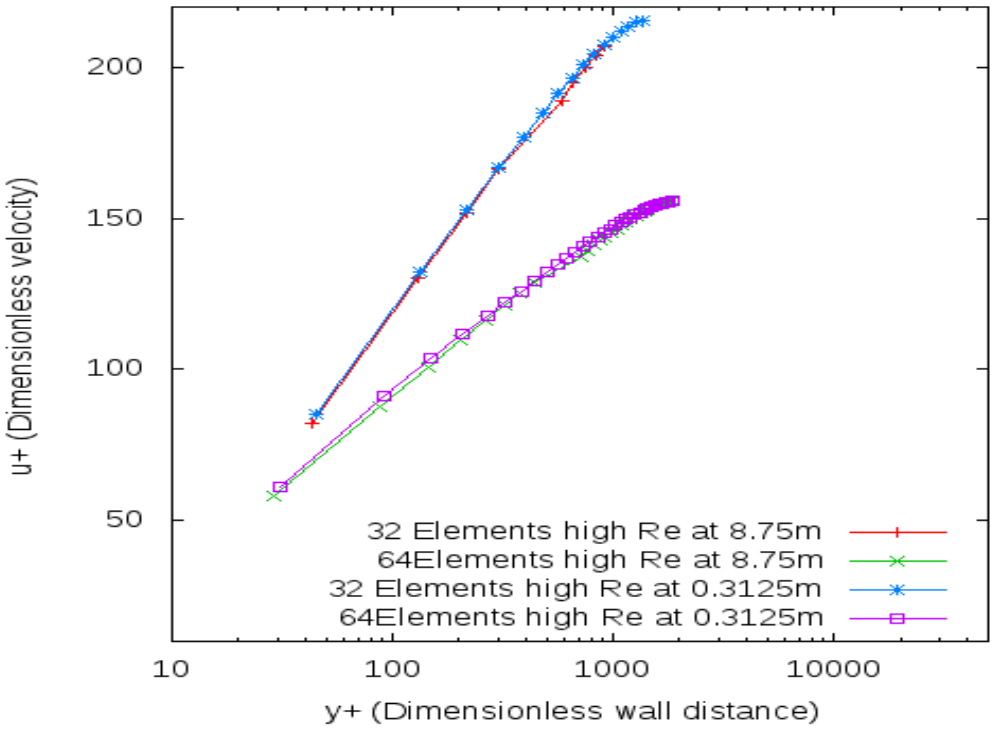

Figure 4.1: Velocity profile in the Van Driest modification.

In the fig. 4.1, it can be noticed that the dimensionless velocities attain a higher value with a coarse discretization of 32 elements compared to a fine discretization of 64 elements for the same value of Reynolds number. The friction velocity which is a scale representative of velocities close to the solid boundary determines the value of u^+. The friction velocity significantly depends on the discretization of the mesh. This might be a possible reason for such behavior of u^+ with different mesh.

Also, it can be noted that the velocity profiles with same discretization and Reynolds number but at different lengths i.e. 0.3125m and 8.75m are found to be nearly similar.

However, the viscous region in the velocity profile of turbulent layer can not be noticed. This is because the viscous layer region occurs for y^+ less than 10. In the fig. 4.1, we do not obtain values of y^+ less than 10 i.e. near the wall. This is because of the uniform mesh of 32 elements used to discretize the flow in space has less elements near the wall. In order to obtain less values of dimensionless wall distance, we need to have more elements near the wall. But an increase in elements will lead to an increase of computational cost. Therefore, to solve the problem a graded mesh is used.

In the graded mesh, the number of elements is not uniformly distributed along the vertical direction of discretization in space. A total number of 32 elements in both directions and a ratio of 1.7 in vertical direction is considered. It has more number of elements near the wall and the height of each element is 1.7 times the height of element exactly below it as shown in the fig. 4.2 below.

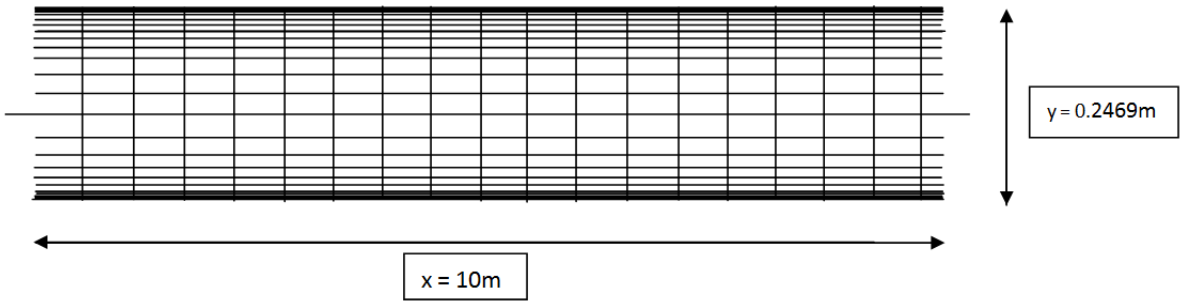

Figure 4.2: Graded mesh discretization in y axis in pipe.

With a graded mesh, we obtain the curves with less values of dimensionless wall distance at different lengths of the pipe as shown in fig. 4.3. In this mesh, more number of elements are located near the wall. Therefore, the wall distance of these elements are less. The formula of dimensionless wall distance is given by:

$$y^+ = \frac{u_t y}{\nu} \tag{4.1}$$

Hence, there is a decrease in the value of y^+ with lesser values of y and the three layers in turbulent flow become visible namely viscous sublayer, log layer and defect layer in fig 4.3.

With higher Reynolds number, the velocities are higher which results in greater values of dimensionless velocities. Therefore, the curves with higher Reynolds number are

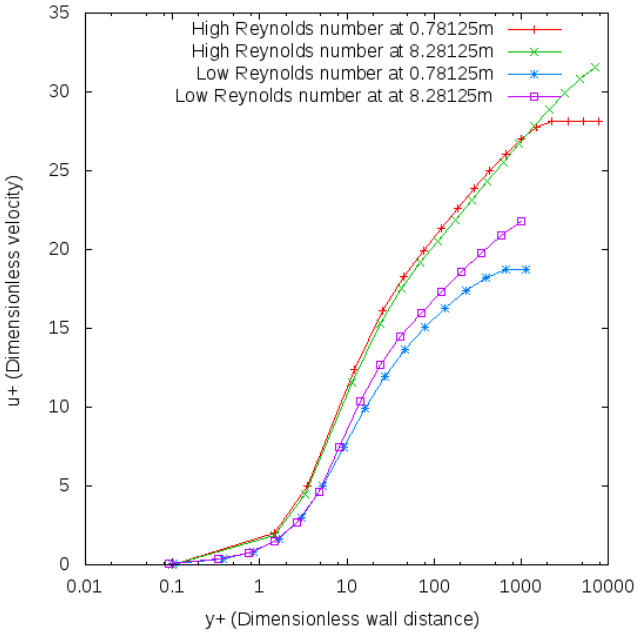

Figure 4.3: Plot obtained by Van Driest modification with the graded mesh of 32 elements and ratio of 1.7.

placed above the curves with low Reynolds number.

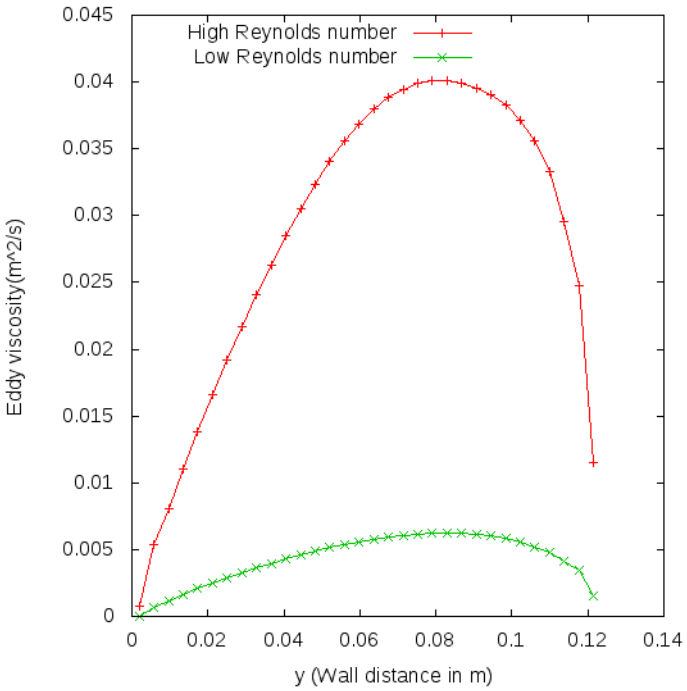

Figure 4.4: Plot of eddy viscosity obtained by Van Driest modification for an uniform mesh of 64 elements.

From the fig. 4.4, it is found that the eddy viscosity follows exponential law and decreases as the wall is approached. However, it increases till a certain point and then decreases till it reaches the mid thickness of the pipe. This behavior can be attributed to the fact that eddy viscosity is dependent on the mixing length and velocity gradient. The velocity gradient initially increases as one moves away from the wall and then decreases as one approaches the center of pipe. Therefore, the eddy viscosity also follows a similar pattern.

4.2.2 Escudier Modification

In the simple mixing length model, the mixing length is overestimated by the expression κy in the outer layer. Therefore, the mixing length is limited to a value of $0.09^{*}\delta$ in Escudier modification.

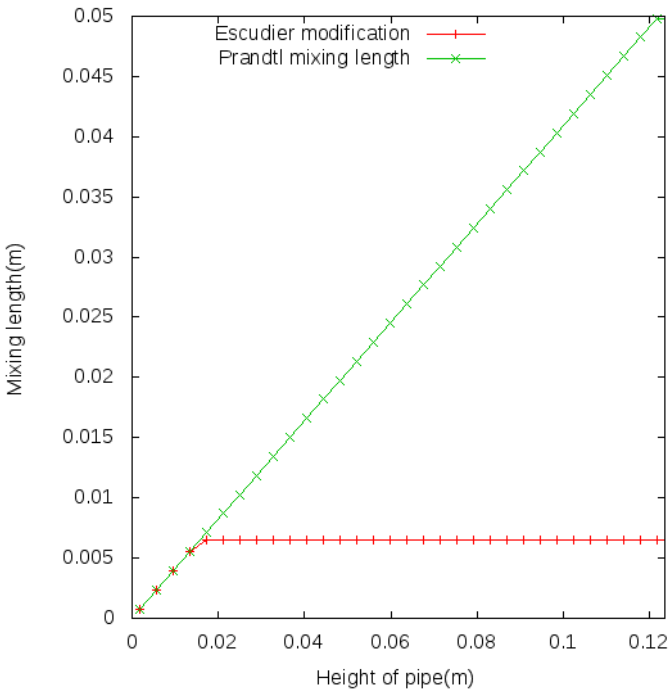

Figure 4.5: Plot of mixing length vs pipe height for high Reynolds number with uniform mesh of 64 elements at 5m.

The boundary layer thickness at a particular point in a flow is constant. Therefore, all mixing length having values more than $0.09^{*}\delta$ will be limited to this value as observed fig. 4.5 at this particular point.

In the fig. 4.6(a) and 4.6(b), we can observe that the Escudier modification with uniform mesh of 64 elements does not give accurate results. However, the Escudier modification with graded mesh gives more accurate solution as compared to uniform

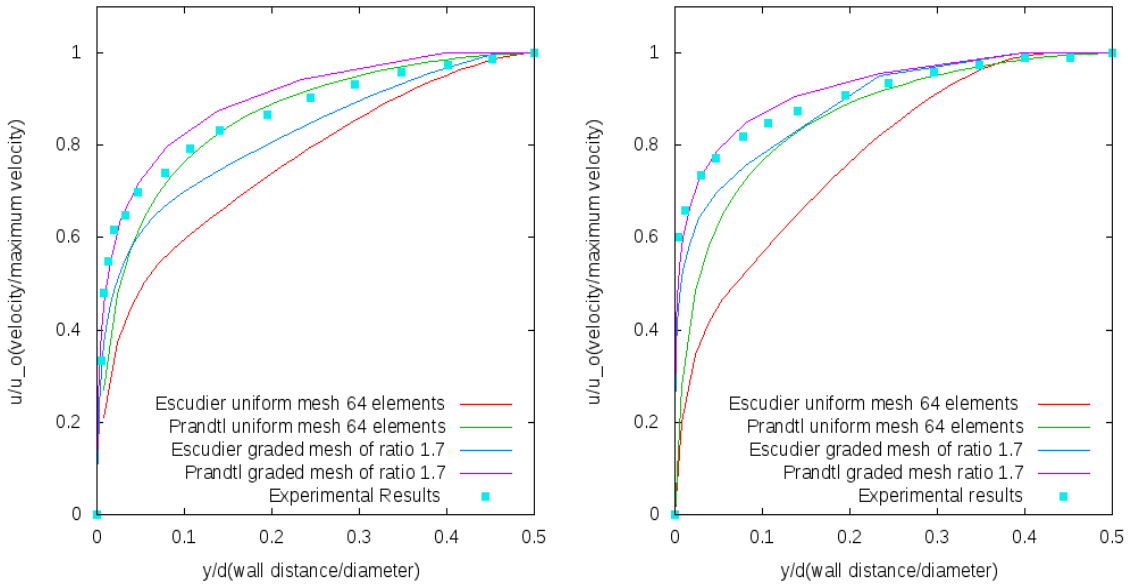

(a) Low Reynolds number

(b) High Reynolds number

Figure 4.6: Comparison of velocity profiles by Prandtl simple and Escudier modification.

mesh. This is because of more number of elements in the graded mesh near the wall which improves the results near the wall region. The same behavior is also observed in the Prandtl mixing length model with uniform mesh and graded mesh respectively. Also, it can be observed that the Prandtl mixing length gives better results as compared to Escudier modification for the experimental setup in consideration.

4.2.3 Corrsin and Kistler and Klebanoff Modification

It was observed through experiments by Corrsin and Kistler that the flow approaching freestream is not fully turbulent in nature. It switches between laminar flow and turbulent flow at irregular intervals. In order to counter the problem, an intermittency function was introduced by Klebanoff. This function reduces the eddy viscosity so as to model this effect.

From the fig. 4.7, it can observed that Klebanoff function has value of one at the wall. This implies that the eddy viscosity has the same value and does not decrease in value at wall. This is justified as the flow is fully laminar near the walls until the freestream is reached. Therefore, the Klebanoff function does not reduce the eddy viscosity in fully turbulent flows.
According to Corrsin and Kistler, as the flow moves away from wall and approaches the freestream from the boundary layer, the switch between laminar and turbulent flow

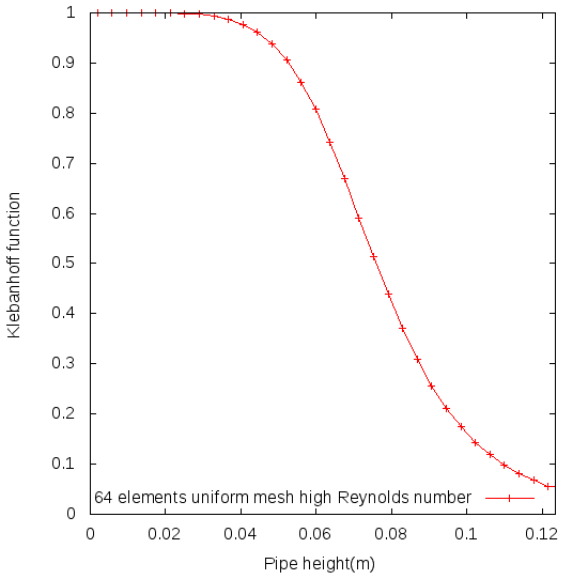

Figure 4.7: Klebanoff function for high Reynolds number in Corrsin and Kistler modification.

occur randomly.

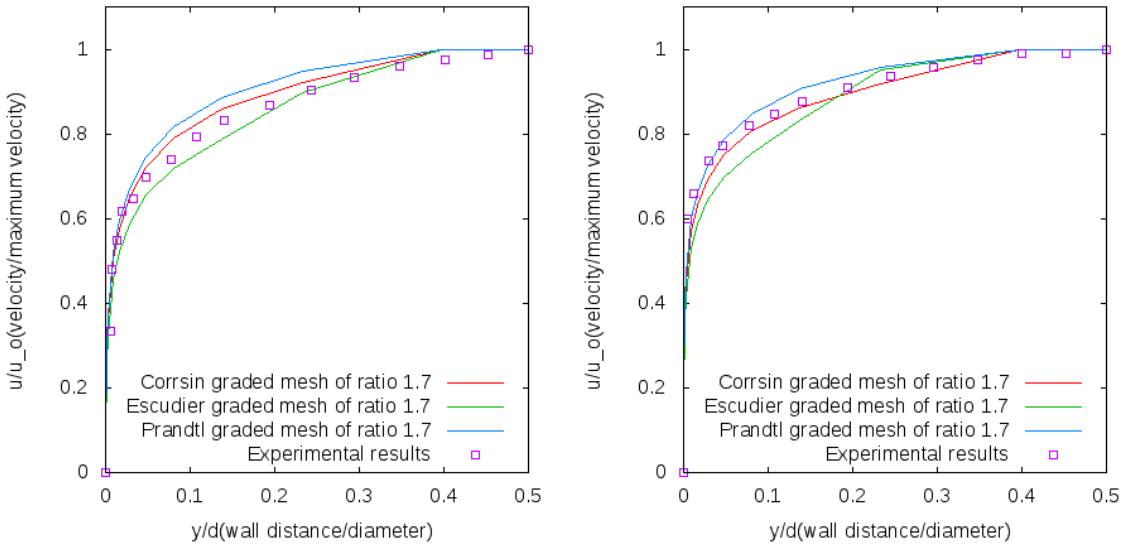

(a) Low Reynolds number

(b) High Reynolds number

Figure 4.8: Velocity profile by Corrsin and Kistler and Klebanoff modification.

However, the flow is still considered to be fully turbulent in previous models. Therefore, the eddy viscosity should be reduced to model this intermittent laminar effect. From the fig. 4.7, it can be noticed that the Klebanoff function decreases as

the freestream is approached. This results in a decrease of the eddy viscosity as the eddy viscosity is multiplied with the Klebanoff function which has a lower value near freestream.

From the figures 4.8(a) and 4.8(b), it can be clearly seen that the Corrsin and Kistler modification reproduces the experimental result best as compared to Prandtl and Escudier modification.
Also it can be noticed that the velocity gradient obtained by Corrsin and Kistler modification is nearly similar to the experimental results as one approaches the freestream. With all these observations, it can be inferred that indeed the flow is intermittently turbulent in the outer turbulent boundary layer. Therefore, the reduction in eddy viscosity by Klebanoff factor taking the laminar flow into account improves the solution.

4.2.4 Cebeci-Smith

The Cebeci-Smith is a two layer algebraic eddy viscosity model consisting of inner and outer regions in the turbulent boundary layer with separate expression for kinematic eddy viscosity in each of these regions.

In the fig. 4.9(a), the inner viscosity is plotted against the wall distance for different mesh sizes. It is worthwhile to note the different values of the viscosities obtained by the different sizes of the meshes used. This behavior can be understood by gaining an insight to the formulation of inner viscosity. The formula for inner viscosity is stated as.

$$\nu_{t_{\text{inner}}} = l_{\text{mix}}^2 \sqrt{\left[\left(\frac{\partial U}{\partial y}\right)^2 + \left(\frac{\partial V}{\partial x}\right)^2\right]} \tag{4.2}$$

Therefore, the inner viscosity depends on the mixing length and velocity gradient. From the fig 4.9(a), it is evident that an increase in the grading of mesh increases is accompanied with a decrease in the value of inner viscosity.
In a graded mesh of ratio 1.7, more elements are distributed near the wall. Therefore, the velocity gradients have comparatively higher values near the wall for graded mesh than uniform mesh as seen in fig. 4.10(a). In a graded mesh, the elements near the wall region have less wall distances. The distances between two elements dy is also very less especially in the region near the wall. This leads to an increase in velocity gradient. The graded mesh have have high values of velocity gradients i.e. (6000-8000)s^{-1} whereas the uniform mesh gives a maximum velocity gradient of 2700s^{-1} as noticed in fig. 4.10(a). However, as the flow moves away from the wall, the velocity gradient of the uniform mesh increases and graded mesh decreases. Thereafter, they become nearly similar to each other. This is due to more number of elements in uniform mesh as compared to graded mesh in the region considerably

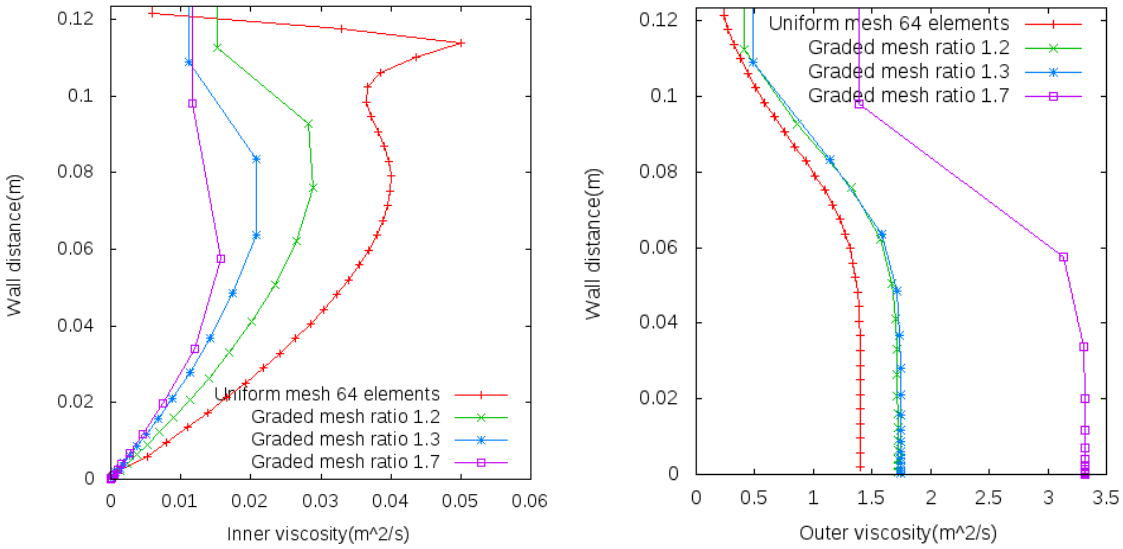

(a) Inner viscosity plot (b) Outer viscosity plot

.

Figure 4.9: Viscosities for High Reynolds number in Cebeci-Smith model

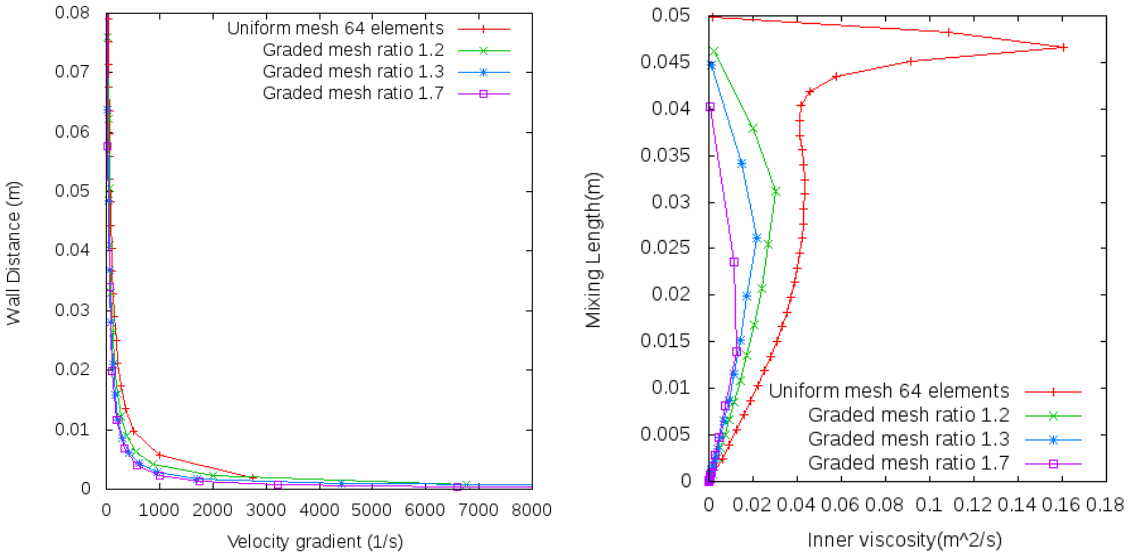

(a) Wall Distance vs velocity gradient (b) Mixing length vs inner viscosity

Figure 4.10: Plot for High Reynolds number in Cebeci-Smith model.

away from wall. These reasons may form the basis for decrease of inner viscosity with an increase in grading of mesh in Cebeci-Smith model.

Also, from the fig. 4.10(b), it is interesting to note the resemblance in behavior

of the inner viscosity with mixing lengths and inner viscosity with wall distance in fig. 4.9(a) for the different mesh considered. This can be explained on the fact that the mixing length is predominantly a function of the velocity gradient and the velocity gradient further determines the behavior of the inner viscosity. So, this might be a possible explanation for obtaining similar curves are obtained in these cases.

In the fig. 4.9(b), the outer viscosity is plotted against the wall distance for different size of meshes at 38.125m. The formula of outer viscosity is stated below.

$$\nu_{t_{\text{outer}}} = \alpha U_e \delta_v^* F_{Kleb}$$

It is observed that the outer viscosity decreases with an increase in the wall distance. This behavior can be attributed to the fact that the outer viscosity depends on the Klebanoff function. In the fig. 4.11(a), it can be clearly seen that the Klebanoff function follows a pattern similar to the outer viscosity when plotted against wall distance.
Also, it is observed that the values of outer viscosity increases with an increase in the grading of the mesh. The results obtained with graded mesh differ a lot from the results obtained with uniform mesh until the free stream is approached. This can be explained on the fact that outer viscosity is directly proportional to the velocity thickness and other parameters. In the fig. 4.11(b), it can be observed that velocity thickness increases with an increase in grading of the mesh. Therefore, the outer viscosity with a uniform mesh has a lower value due to lower value of the velocity thickness. Therefore, these reasons might form the basis for such behavior of the outer viscosity.

In the fig. 4.12, the eddy viscosity is plotted against the wall distance. Initially, the eddy viscosity adopts the values of inner viscosity. The point at which the inner viscosity becomes equal to the outer viscosity, the eddy viscosity switches to outer viscosity. Upon comparison of the curves for inner viscosity and outer viscosity, it can be found that the eddy viscosity takes the value of outer viscosity as compared to inner viscosity after a certain wall distance.

In the fig. 4.13(a) and 4.13(b), the dimensionless wall distance is plotted against the dimensionless velocity. There occurs a deviation near the end of the boundary layer as can be seen from the plot. This is because, such a defect from the log-law in the outer region of the boundary layer is also observed in various experimental results. Thus, this region is named as 'defect layer'. As its name implies, the logarithmic profile, so that there is a defect.
Also, as mentioned earlier, with an increase in grading of the mesh, the region of curve near the wall is obtained. Furthermore, it is noticed that the curves of higher Reynolds number are placed above the curves with lower Reynolds number.
This can be attributed to the higher values of dimensionless velocity with higher

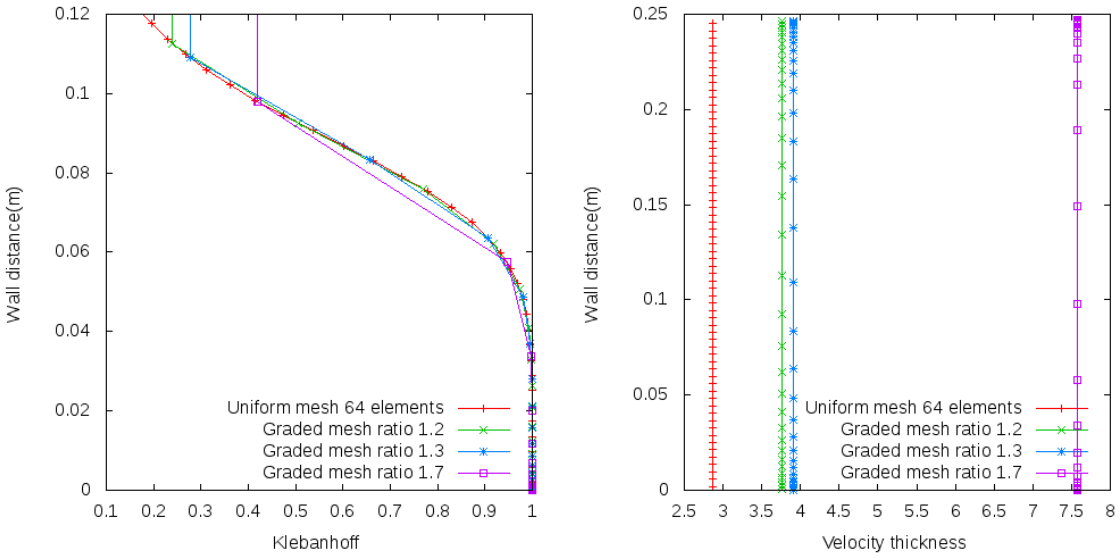

(a) Klebanoff funciton (b) Velocity thickness at 38.125m length of pipe

Figure 4.11: Plot for High Reynolds number in Cebeci-Smith model

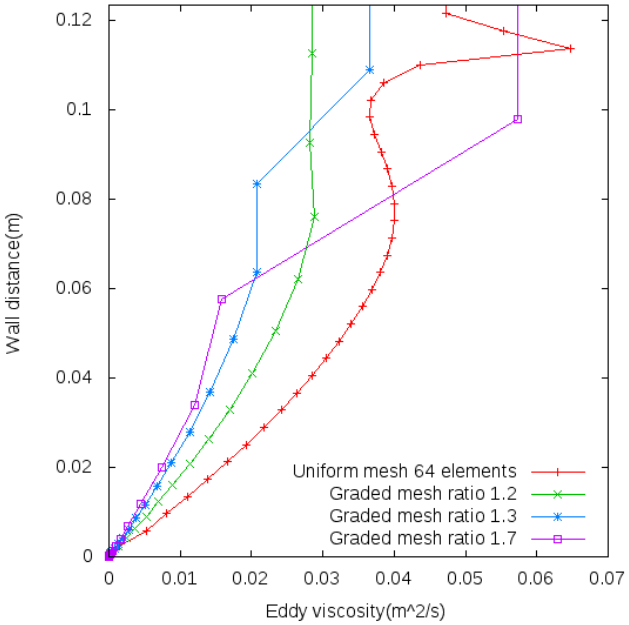

Figure 4.12: Kinematic eddy viscosity plot with high Reynolds number in Cebeci-Smith model.

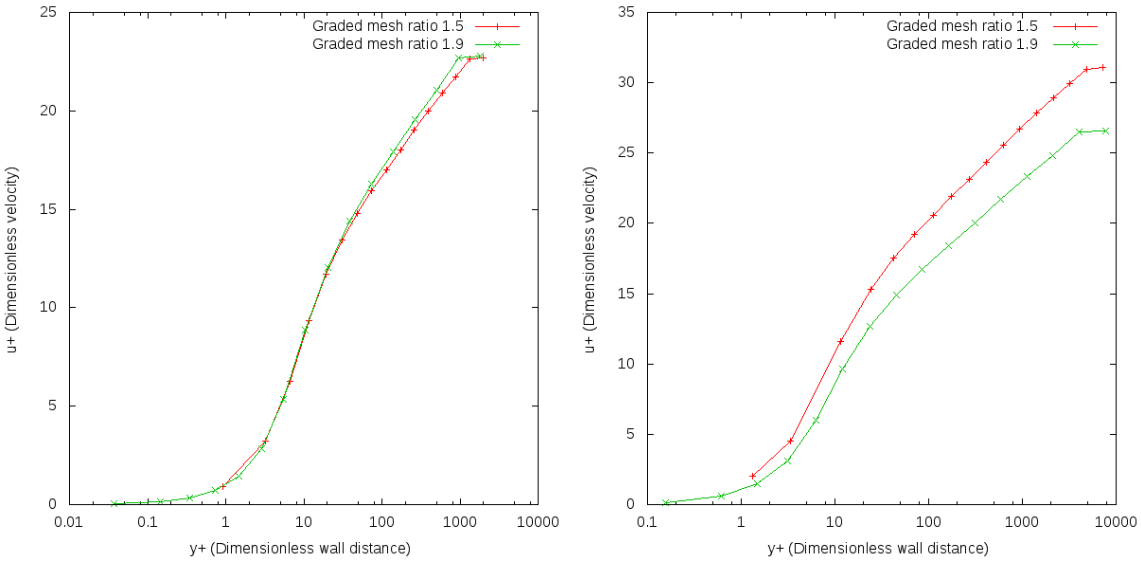

(a) Low Reynolds number (b) High Reynolds number

Figure 4.13: Logarithmic law for velocity at 19m.

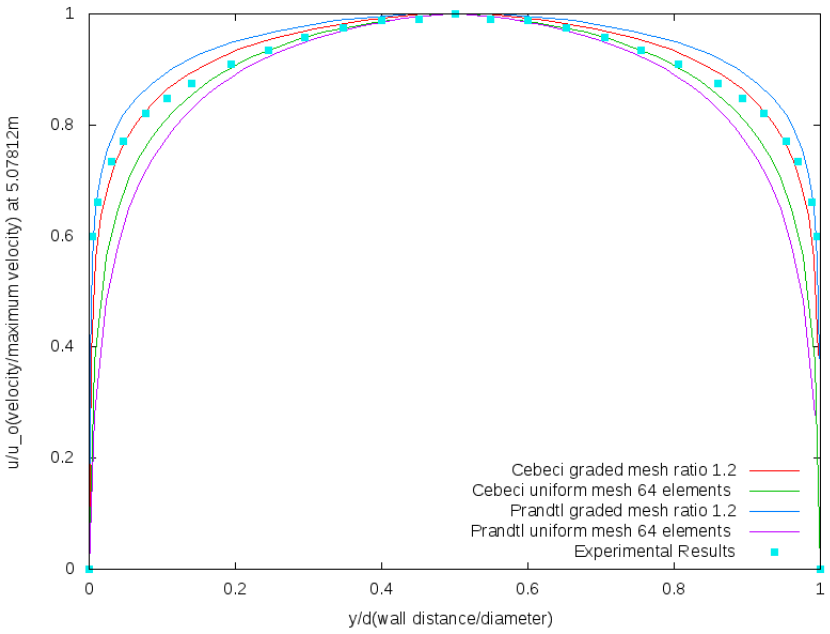

Figure 4.14: Velocity profile for high Reynolds number.

Reynolds number as compared to lower Reynolds number at the same wall distances.

In the fig. 4.14, it can be observed that the Cebeci-Smith model produces more accurate results as compared to the simple Prandtl mixing length model. This is because it uses

inner viscosity and outer viscosity which causes better reproduction of velocities with the exact solution. However, the results obtained by Cebeci-Smith model assume more similarity with the experimental results after grading the mesh by a factor of 1.2.

4.2.5 Baldwin-Lomax

In this section, some of the properties of the model are highlighted to explain certain behavior of the outputs. The input values as discussed earlier are considered for producing outputs by the Baldwin-Lomax model.

In the fig. 4.15(a), it can be observed that the inner viscosity follows a pattern similar to the Cebeci-Smith model i.e. it decreases upon increasing the grading of mesh.

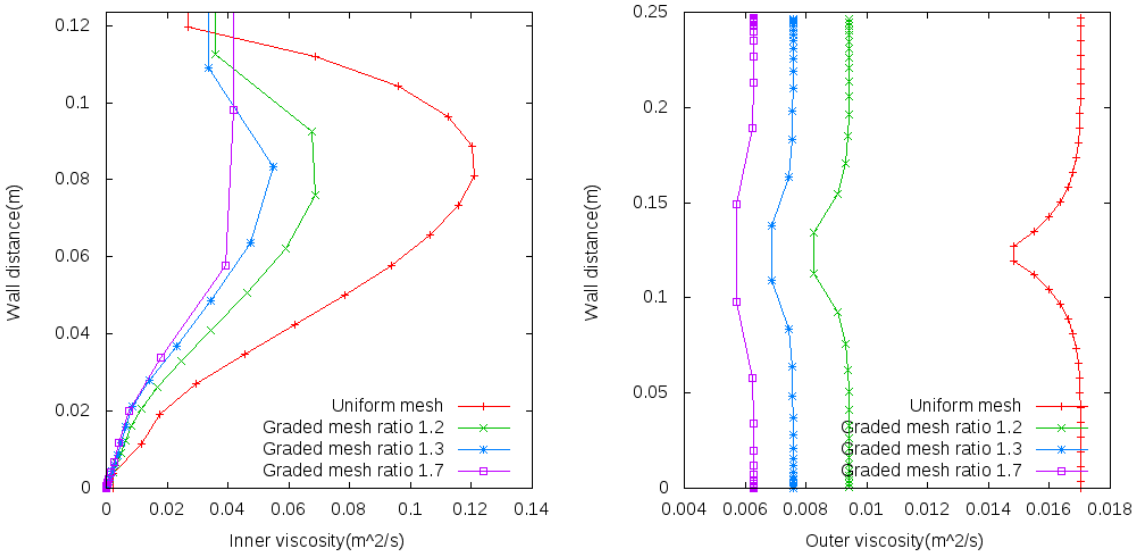

(a) Inner viscosity plot

(b) Outer viscosity plot

Figure 4.15: Viscosities for High Reynolds number in Baldwin-Lomax model

This can explained on the basis that inner viscosity in both the models have same formulation. The reason for the similar behavior of the inner viscosity explained in the Cebeci-Smith also holds true in this case too.

In the fig. 4.15(b), it is noticed that the outer viscosity decreases upon increasing the grading in mesh. In other words, an increase in number of elements near the wall produces relatively low values of outer viscosity. This can be better understood better by following the computation steps in the Baldwin-Lomax model. With higher grading, the elements and the corresponding wall distances are of small size in the region near the wall. Therefore, the product of mixing length and vorticity which

determines the value of F_{max} also attains lesser values.

$$F_{\max} = \frac{1}{\kappa}\left(\max(l_{\text{mix}}|\omega|)\right)$$

This might be a possible explanation for the decrease in value of $l_{\text{mix}}|\omega|$ with an increase in grading of the mesh as noticed in fig. 4.16(a). But, the y_{max} being the wall distance at which the F_{max} attains maximum value remains constant in all the cases.

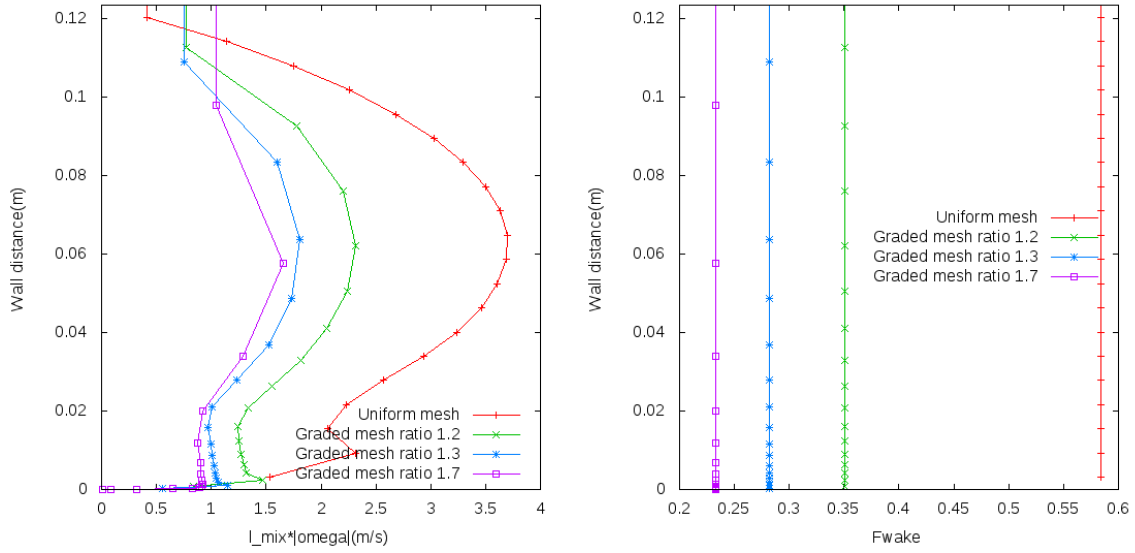

(a) $l_{mix}|\omega|$ plot (b) F_{wake} plot

Figure 4.16: Plots for High Reynolds number in Baldwin-Lomax model

$$F_{\text{wake}} = \min\left(y_{\max}F_{\max};\ C_{\text{wk}}y_{\max}U_{\text{dif}}^2/F_{\max}\right)$$
$$\nu_{t_{\text{outer}}} = \alpha C_{\text{cp}}F_{\text{Wake}}F_{\text{Kleb}}(y; y_{\max}/C_{\text{Kleb}})$$

Now, the F_{max} so computed further determines the value of F_{wake}.
So, it is again noticed that the value of the F_{wake} decreases as the grading of the mesh increases in the fig. 4.14(b). Finally, the outer viscosity being proportional to F_{wake} also decreases upon increasing the grading in mesh.

In the fig. 4.17(a), the eddy viscosities are plotted against the wall distances. The eddy viscosity makes a change in adopting values from inner viscosity to the outer viscosity at the distance y_m where both the viscosities attain similar values as mentioned earlier. The y_m can be determined graphically by superimposition of the outer viscosity curve on the inner viscosity curve as shown in fig. 4.17(b). Thereafter, y_m can be computed as the distance of point where the curve changes its shape significantly from the wall. Moreover, the curve of eddy viscosity obtained in current case is in total agreement

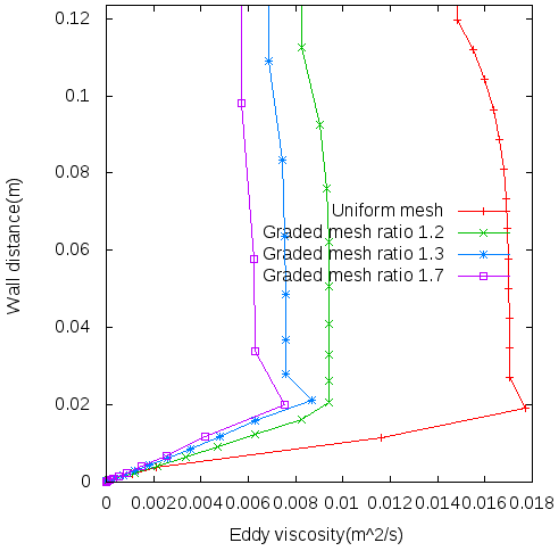

(a) Plot of Kinematic eddy viscosity

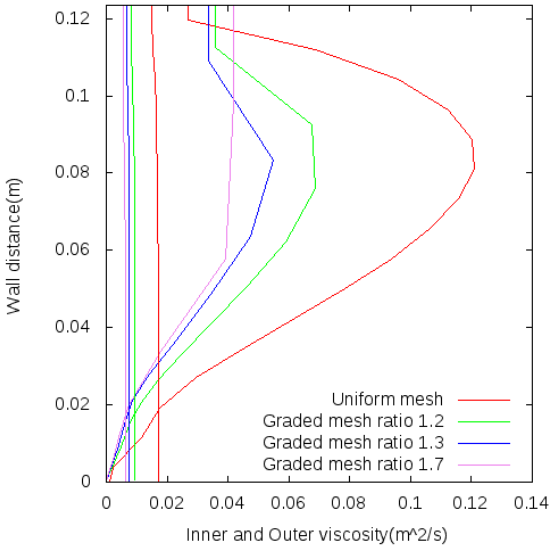

(b) Superimposed plot of inner and outer viscosity

Figure 4.17: Viscosities for High Reynolds number in Baldwin-Lomax model

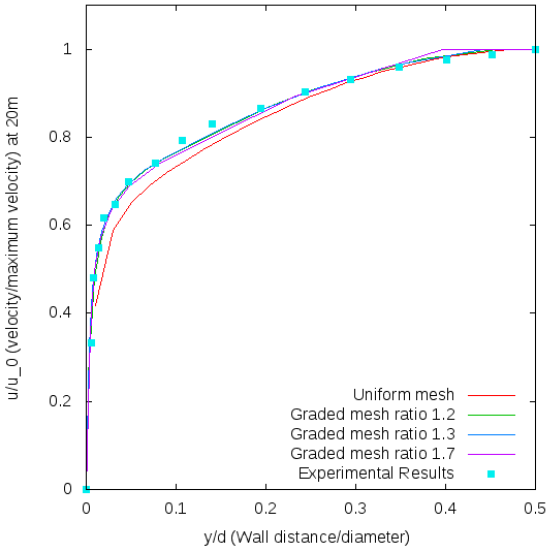

(a) Low Reynolds number

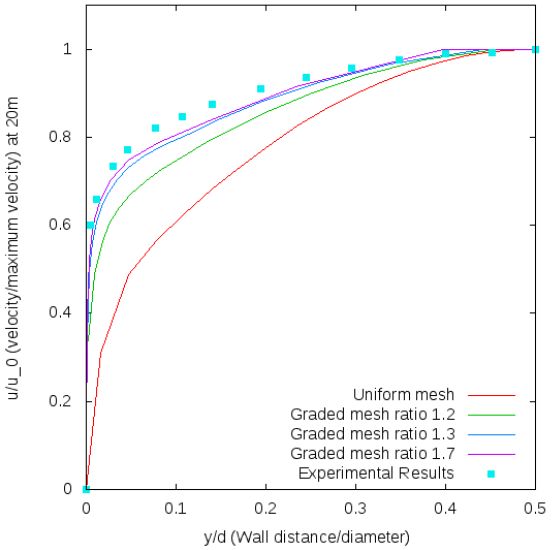

(b) High Reynolds number

Figure 4.18: Velocity profiles in Baldwin-Lomax model

with the curve of Baldwin-Lomax model.

In the fig. 4.18(a) and fig. 4.18(b), it can be seen that the velocity profile improves

more towards the experimental results as the grading of mesh is increased.
With a higher grading, more elements are located near the wall. Therefore, the velocity profile with graded mesh near the wall are more accurate as compared to the uniform mesh. Also, the overall velocity profile tends to have more similarity with the experimental results.
Also, it is necessary to note that the Cebeci-Smith model as discussed earlier renders accurate velocity profiles with a grading of 1.2 as compared to Baldwin-Lomax with a grading of 1.7.

4.3 Comparative Analysis

The objective of this section is to draw conclusions by making a comparison of the results obtained by all the models.

4.3.1 All Models

The velocity profile of all the five models considered in the current study are analyzed. The details of the input considered are similar to that discussed earlier.

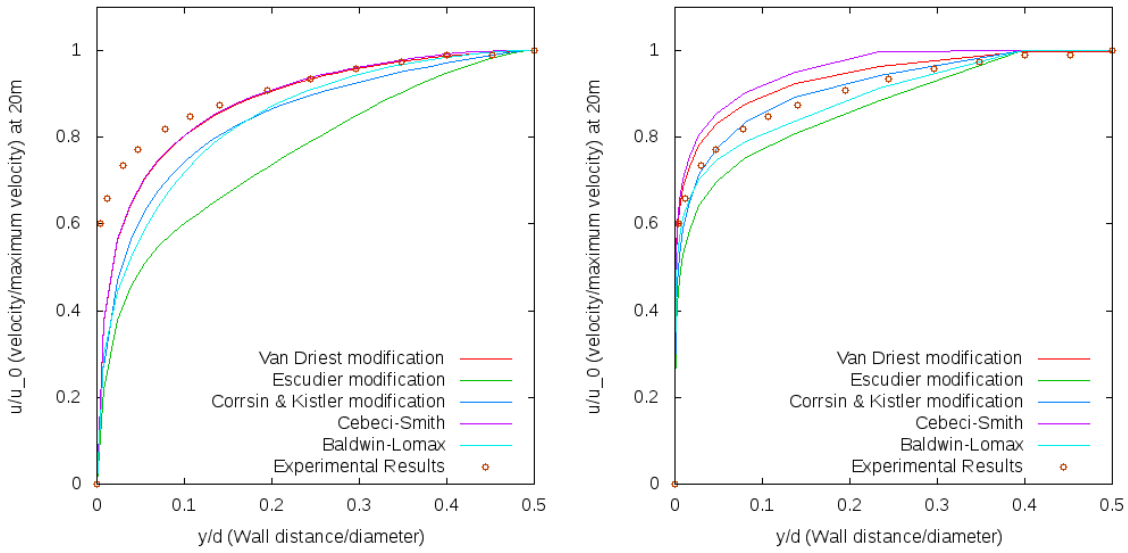

(a) Uniform mesh of 64 elements

(b) Graded mesh of ratio 1.7

Figure 4.19: Velocity profiles for high Reynolds number

In the plot 4.19(a),the velocity profiles obtained by all the method are compared for high Reynolds number using an uniform mesh of elements. It is observed that the Van Driest and Cebeci-Smith render results that are close to the experimental solution as compared to other methods. As discussed earlier, the results obtained by Escudier

and Baldwin Lomax differ a lot from experimental solution for the uniform mesh. However, the Corrsin and Kistler modification gives better result as compared to the Escudier and Baldwin-Lomax. This is due to the inclusion of intermittency factor in the model which improves the result.

On a broader scale, the results obtained with uniform mesh by all the methods do not produce accurate solution. The deviation from the experimental solution begins as the flow begins to move away from the wall. This is because of less concentration of elements near the wall. With high Reynolds number, there is development of the turbulent boundary layer in addition to laminar boundary layer near the wall.
The turbulent boundary layer consists of regions marked with irrotational flows and vortices. These vortices pump the low momentum fluid near the wall in upward direction. This upwelling generates Reynolds shear stresses. Moreover, there is occurrence of intermittent characteristics in the upper portion of the turbulent boundary layer. Therefore, more number of elements are required near the wall to simulate these behaviors and obtain relatively better results.

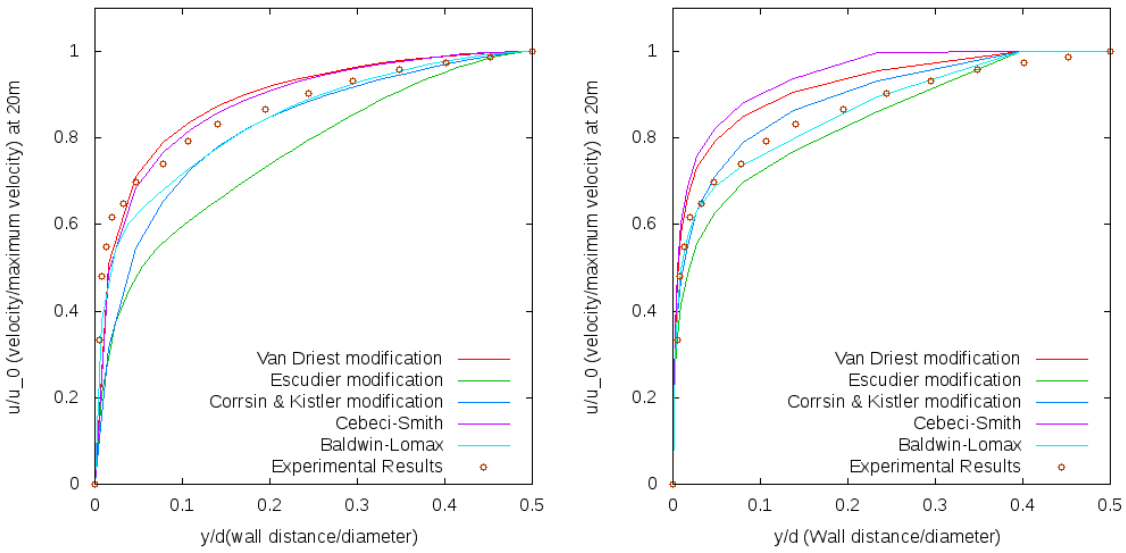

(a) Uniform mesh of 64 elements

(b) Graded mesh of ratio 1.7

Figure 4.20: Velocity profiles for low Reynolds number

In the fig. 4.19(b), a graded mesh with ratio of 1.7 is used for comparison of the velocity profiles for all the models under consideration with high Reynolds number. This mesh has more number of elements distributed near the wall. From the fig. 4.19(b), it can observed that the results obtained by the graded mesh for all the models are comparatively better than the previous case. Baldwin-Lomax and Corrsin-Kistler

render the best results among all the models for graded mesh.

In the fig. 4.20(a), an uniform mesh is used to plot the velocity profiles for the models with low Reynolds number. The results obtained by Cebeci-Smith and Van Driest modification are more close to the experimental solution as compared to other methods. The velocity profile of Escudier modification has a lot of deviation from the experimental solution. This might be attributed to the fact that it is the simple mixing length model with the mixing length limited to a value of 0.09δ. It does not include the intermittency property of flow as it approaches the free stream, inner and outer viscosities for turbulent behavior. The results produced by Baldwin-Lomax are more accurate in the region near the wall and freestream. However, the solution by Corrsin and Kistler modification are more close to the experimental solution near the freestream.

In the fig. 4.20(b), a graded mesh with a ratio of 1.7 is used for the same low Reynolds number. With a higher concentration of elements near the wall in the mesh, the velocity profile is nearly similar to the experimental values near the wall for all the models except the Van Driest and Cebeci-Smith model. Therefore, the results obtained by graded mesh are comparatively better than the uniform mesh. Again, the Baldwin-Lomax and Corrsin-Kistler render the best results among all the models.

4.3.2 Logarithmic Velocity profile

In this section, the logarithmic law of wall is obtained and analyzed for all the models under consideration. In the fig. 4.21(a) and 4.21(b), the logarithmic velocity profile of all the models in current study are plotted. It can be observed that the curves of Baldwin-Lomax, Van Driest and Cebeci-Smith are nearly identical till the outer layer of the log layer. Similar behavior is also observed for the Escudier modification and Corrsin and Kistler modification.
On a general note, the Baldwin-Lomax reproduces the experimental result best among all the models for both the Reynolds number. Even, the results obtained by Van-Driest and Cebeci-Smith are very close to experimental solution but they deviate from the experimental solution at higher velocities as noticed in the graphs.
Also, it is worthwhile to note that dimensionless velocities obtained by the Cebeci-Smith, Van Driest and Baldwin-Lomax model are more than Escudier modification and Corrsin and Kistler modifications.

4.3.3 Staggered and Regular Grid

In this section, comparison are made between staggered grid and Box method for the Van Driest modification and the Baldwin-Lomax model.

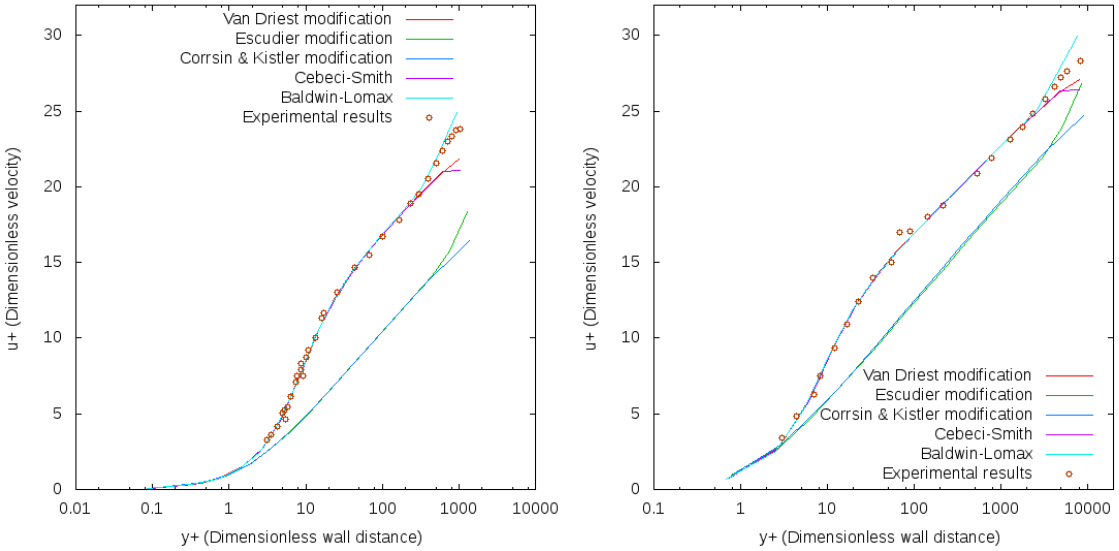

(a) Low Reynolds number (b) High Reynolds number

Figure 4.21: Logarithmic velocity profiles.

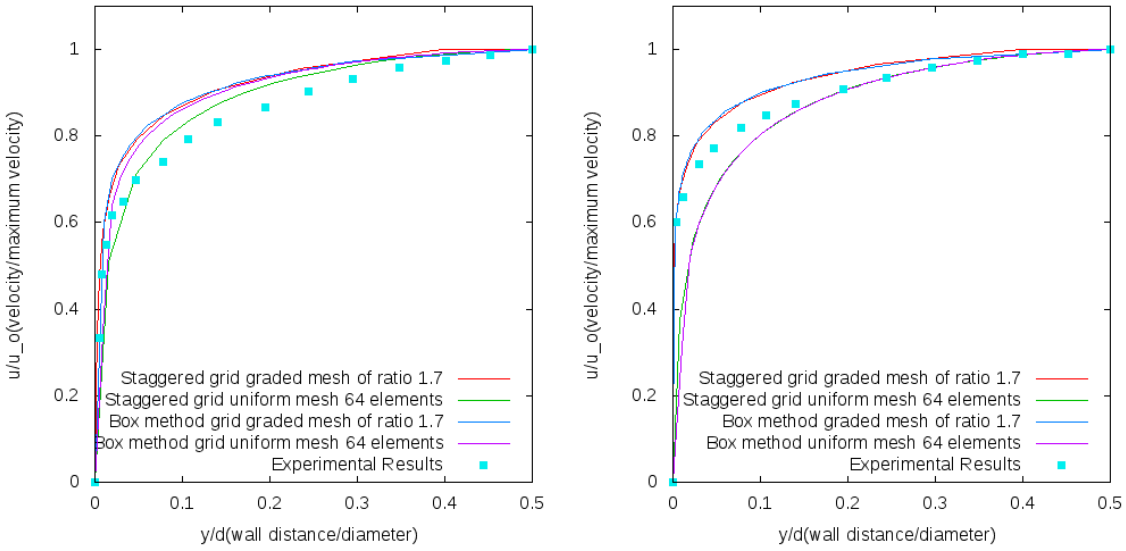

(a) Low Reynolds number (b) High Reynolds number

Figure 4.22: Velocity profiles comparison between staggered Grid and Box method for Van Driest modification.

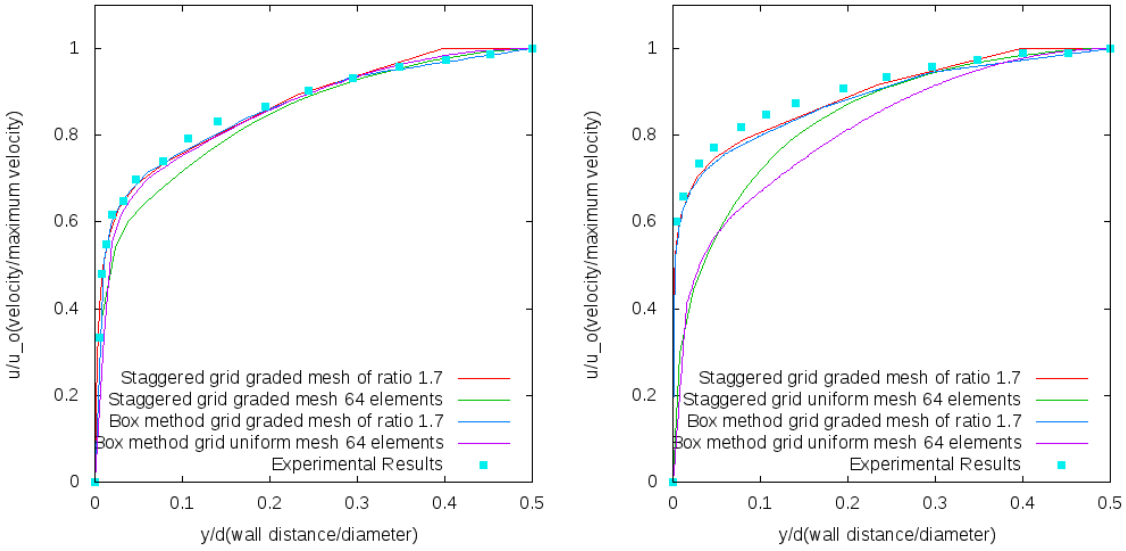

(a) Low Reynolds number

(b) High Reynolds number

Figure 4.23: Velocity profiles comparison between staggered Grid and Box method for Baldwin-Lomax model.

In the fig 4.22(a) and 4.22(b), the velocity profiles are compared between box method and staggered grid for the Van Driest modification. In an uniform mesh, with a low Reynolds number, it can be observed that the velocity profile with a staggered grid is more accurate than the box method upon comparison with the experimental results. Even, with a uniform mesh and high Reynolds number, the velocity profile obtained by staggered grid is better than box method especially near the wall. However, the velocity profile obtained with graded mesh are nearly similar for the staggered grid and box method.

In the fig. 4.23(a) and 4.23(b), the velocity profiles are analyzed between box method and staggered grid for the Baldwin-Lomax model. In an uniform mesh, with low and high Reynolds number, the velocity profile with staggered grid renders result that is more close to the experimental results especially near the wall as compared to box method. But again, with a graded mesh, the results obtained for staggered grid and box method are nearly identical.

The advantage of staggered grids are more accurate pressure gradient and prevention of the pressure oscillations. In the regular grid of box method, the pressure gradient is approximated with two alternate grid points when a central difference scheme is used. Therefore, a wavy pressure field is felt like a uniform pressure field by the momentum equation. However, in a staggered grid, the pressure gradient is approximated by the difference of pressures between two adjacent grid points. So, the pressure having

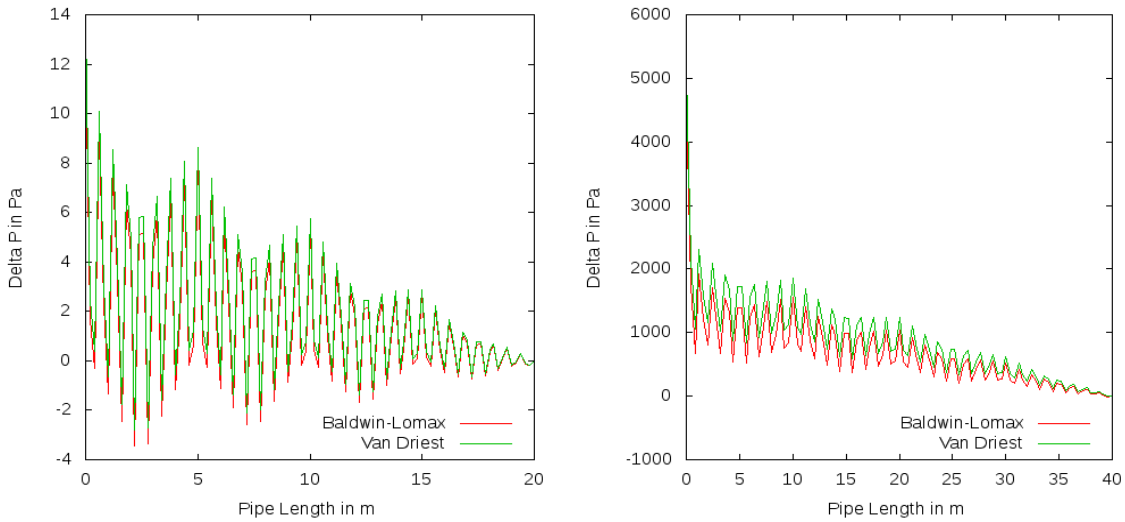

(a) Low Reynolds number (b) High Reynolds number

Figure 4.24: Plot of Pressure with Pipe length for box method.

oscillatory behavior does not become an uniform pressure field and could not become a possible solution. The discretized continuity equation given by:

$$\frac{u^{n+1}_{i+1/2,j} - u^{n+1}_{i-1/2,j}}{\Delta x} + \frac{v^{n+1}_{i,j+1/2} - v^{n+1}_{i,j-1/2}}{\Delta y} = 0; \tag{4.3}$$

contains differences of the adjacent velocity components which prevents a wavy velocity field from the satisfying the continuity equation. Therefore, the accuracy of the solution increases with the use of a staggered grid.
In the fig. 4.24(a) and 4.24(b), it can be seen that the pressure oscillations occur in the box method for both Van driest and Baldwin-Lomax model respectively. However, in fig. 4.25(a) and 4.25(b), it is observed that there is no pressure oscillations with the staggered grid.

The staggered grid is known to prevent any occurrence of pressure oscillations. Staggered grid automatically couples the grid scale to pressure to the remainder of the solution. Therefore, it does not suffer from the problem of pressure oscillation.

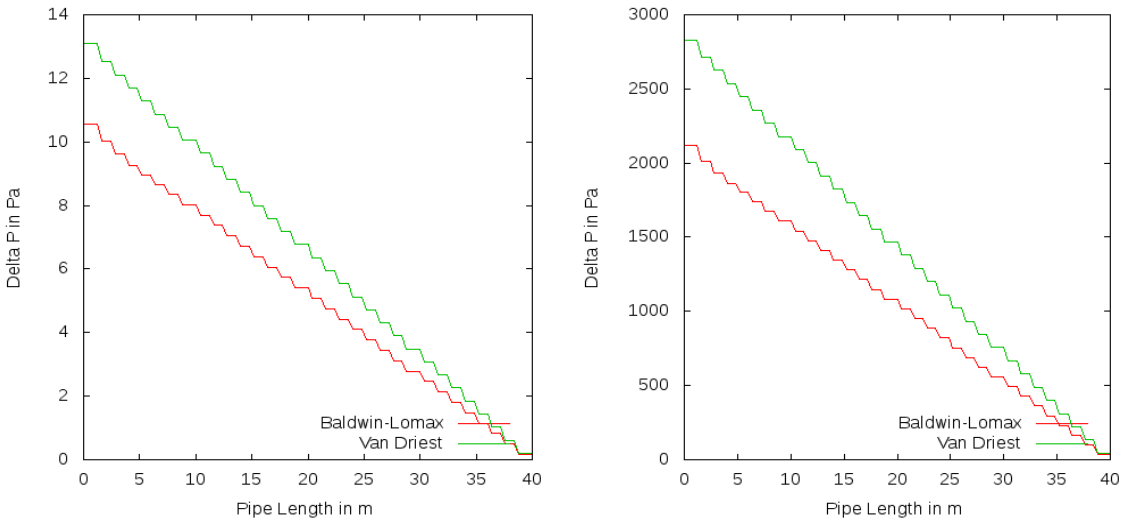

(a) Low Reynolds number

(b) High Reynolds number

Figure 4.25: Plot of Pressure with Pipe length for Staggered grid.

4.3.4 Running Time

The running time of the algebraic models are compared for same set of input values as discussed earlier but with an uniform mesh of 32 elements and Reynolds number of 500 000.

Model	**Time(s)**
Prandtl	145.05
Van Driest	143.33
Escudier	133.22
Corrsin and Kistler	144.51
Cebeci-Smith	234.58
Baldwin-Lomax	249.91

The Cebeci-Smith and Baldwin-Lomax models are found to take relatively more running time in comparison with the Prandtl mixing length and its three modifications. The Cebeci-Smith and Baldwin-Lomax models have more additional parameters in computation of eddy viscosities as compared to the Prandtl mixing length, Van Driest, Escudier and Corrsin and Kistler modifications. Therefore, both the models are computationally more expensive and have relatively more running time.

Chapter 5

Summary And Outlook

The trouble with research is that it tells you what people were thinking about yesterday, not tomorrow. It's like driving a car using a rear view mirror.

- Bernard Loomis -

5.1 Implementation and Analysis

The prime objective of the current study is the modeling and analysis of turbulence in free flowing gas phase. In this regard, five different models of turbulence were implemented through the framework of DuMu^x and using a staggered grid.

Initially, the analysis was performed for each of the models individually. The characteristic features of the models were highlighted in the analysis. It included behavior of the parameters like mixing length, inner viscosity, outer viscosity and Klebanoff function. Further, an improvement in the accuracy of the results was noticed upon progressing from Van Driest modification to Baldwin-Lomax model. Firstly, in the Van Driest model, the exponential law of eddy viscosity was put into practice. Secondly, in the Escudier modification, the restriction on the mixing length was employed. Thirdly, in the Corrsin and Kistler and Klebanoff modification, the intermittency of turbulent flow as it approaches free stream was applied through the Klebanoff function. This resulted in more accurate results upon comparing with the experimental values. Fourthly, the Cebeci-Smith model was also executed with the inner and outer viscosities. Finally, the Baldwin-Lomax model consisting of additional parameters was also realized.

Furthermore, all the models were analyzed in a combined manner. The models like Baldwin-Lomax and Corrsin and Kistler modification performed the best among all the models under consideration. Moreover, the logarithmic velocity profile of all the models were analyzed too. Finally, a comparison was made between the staggered grid and the box method especially for the Van Driest modification and Baldwin-Lomax

models. It was found that the pressure oscillations observed in box method were absent in the staggered grid. Also, the velocity oscillations were also reduced in the staggered grid which lead to more stable results. Additionally, it was found that the results obtained for low Reynolds number were relatively more accurate than the ones obtained with high Reynolds number. The analysis was carried out with different grading of the mesh and an attempt was made to understand the observed behaviors.

On a general note, it can be inferred that the algebraic models give good results for simple flows. The algebraic models are fast and robust in computation. They require information pertaining to the boundary layer properties.

5.2 Outlook

A possible field of research will be devising and implementing a method to model separated flows by Cebeci-Smith and Baldwin-Lomax models. As the boundary layer separates, it is necessary to solve the full Reynolds-averaged Navier-Stokes equation, which includes all components of Reynolds stress tensor. Several schemes like MacCormack schemes which are second order accurate in space and time can be used for this purpose. This scheme involves a predictor step and a corrector step. Other schemes like Jameson and Mavriplis can be used. It is a symmetrical scheme in which discretization is performed by a Runge-Kutta method having five stages. It is a robust method which gives good accuracy and prediction of separation region in modeling with Cebeci-Smith and Baldwin-Lomax [8].
Another approach that can be used to calculate flows with separation region is by a combination of the Baldwin-Lomax and Smagorinsky turbulence models. The Baldwin-Lomax model can be used near the wall as it gives good result near the walls. Then, from the end of inner layer to the core flow region, a mix of Baldwin-Lomax and Smagorinsky model can be used for modeling of the flow.
With these implementations, it would be important to study different fields like modeling the water hammer and flow over airfoil.

Another possibility of future work can be computations of results for different experimental setup. The results so obtained can be compared with the experimental results for the similar experimental setup.

Bibliography

[1] http://www.brookfieldengineering.com/education/what-is-viscosity.asp.

[2] http://www.cfm.brown.edu/people/gk/chap6/node15.html.

[3] http://www.mathematik.uni-dortmund.de/ kuzmin/cfdintro/lecture8.pdf.

[4] Dumux homepage. http://www.dumux.org/.

[5] Aerospace Mechanical and Mechatronic Engineering. Aerodynamics for students. University of Sydney, 2005.

[6] Celik, I. B. Introductory turbulence modeling. West Virginia university , Mechanical & Aerospace Engineering Department, P.O. Box 6106, Morgantown, WV 26506-6106, December 1999.

[7] Department of hydromechanics and hydrosystems modelling, Stuttgart. *Dumux handbook*. http://dumux.org.

[8] Edisson Savio de Goes Maciel. Turbulent flow simulations using the Maccormack and the Jameson and Mavriplis algorithm coupled with the Cebeci Smith and the Baldwin Lomax model in the three dimensions. Engineering Applications of Computational Fluid Mechanics, Vol. 1, No. 3, pp. 147-163 (2007), 2007.

[9] Glenn research center, National Aeronautics and Space Adminstration, USA. Boundary layer.

[10] Imperial College London. Research: Turbulent flow modelling and simulation. http://www3.imperial.ac.uk/tfms/turbulentflowmodelling.

[11] Kenryk Kudela. Viscous flow in pipe.

[12] Knopp, T. Boundary layer flows, the logarithmic law of the wall ,mixing length model for turbulent viscosity. DLR Göttingen, November 2008.

[13] McDonough, J. Lectures in elementary fluid dynamics: Physics, mathematics and application. *Deaprtment of Mechanical Engineering and Mathematics, University of kentucky, Lexington, KY 40506-0503*, S. 163, 2009.

[14] National Programme on Technology Enhanced Learning. Fluid mechanics tutorial no. 3. Ministry of HRD, Government of India.

[15] National Programme on Technology Enhanced learning, Ministry of HRD, Government of India. Lecture -1: Fundamental aspects, viscous incompressible flow.

[16] Tu, Jiyuan, and Inthavong, Kiao, and Ahmadi, Goodarz. *Computational fluid and particle dynamics in the human respiratory system*. Springer Dordrecht, 2013.

[17] Veldman, A. *Boundary layers in fluid Dynamics*. Faculty of mathematics and natural sciences, 2011-2012.

[18] Versteeg, H. and Malalasekera, W. *An Introduction to Computational Fluid Dynamics: The Finite Volume Method*. Pearson Education Limited, 2007.

[19] Wagner, H. and Sagaut. *Large-Eddy Simulation for Acoustics*. Cambridge University Press.

[20] Widera, P. Study of sediment transport processess using reynolds avergaed navierstokes and large eddy simulation. *PhD Thesis, Faculty of Engineering, Vrije Universiteit Brussel*, S. 205, 2011.

[21] Wikipedia. Cebecismith model, December 2013.

[22] Wikipedia. Mixing length model. Wikipedia, November 2013.

[23] Wikipedia. Turbulence modeling. 2013.

[24] Wikipedia. Boundary layer. February 2014.

[25] Wikipedia. Reynolds-averaged navierstokes equations, March 2014.

[26] Wikipedia. Turbulence, May 2014.

[27] Wilcox, D. *Turbulence Modeling for CFD: Text*. Turbulence Modeling for CFD. DCW Industries, Incorporated, 2006.